NASA TECHNICAL NOTE

NASA TN D-4872

C. 1

NASA TN D-4872

LATERAL VIBRATION CHARACTERISTICS OF A 1/40-SCALE DYNAMIC MODEL OF APOLLO-SATURN V LAUNCH VEHICLE

by Earl C. Steeves and John J. Catherines

Langley Research Center
Langley Station, Hampton, Va.

NATIONAL AERONAUTICS AND SPACE ADMINISTRATION • WASHINGTON, D. C. • NOVEMBER 1968

NASA TN D-4872

LATERAL VIBRATION CHARACTERISTICS OF A 1/40-SCALE DYNAMIC MODEL OF APOLLO-SATURN V LAUNCH VEHICLE

By Earl C. Steeves and John J. Catherines

Langley Research Center
Langley Station, Hampton, Va.

NATIONAL AERONAUTICS AND SPACE ADMINISTRATION

For sale by the Clearinghouse for Federal Scientific and Technical Information
Springfield, Virginia 22151 – CFSTI price $3.00

LATERAL VIBRATION CHARACTERISTICS OF A 1/40-SCALE DYNAMIC MODEL OF APOLLO-SATURN V LAUNCH VEHICLE

By Earl C. Steeves and John J. Catherines
Langley Research Center

SUMMARY

Analytical and experimental investigations of the lateral vibration characteristics of a dynamically similar 1/40-scale model of the Apollo-Saturn V launch vehicle have been performed. A brief description of the model is given and the procedures used in the tests and reduction of the data are discussed. The idealization of the model and method of analysis are presented. The free-free natural frequencies and corresponding mode shapes are presented for weights corresponding to several flight times including staged configurations. In addition, cantilever results and experimental modal damping values are presented.

In general, good agreement was found between analytical and experimental results; thus the idealization is validated and the beam idealization adequately represents the motion of the model over the frequency range of the investigation. On comparing the frequency of the 1/40-scale model with those of a 1/10-scale replica model, good agreement is found for the first three modes. This comparison indicates that the degree of relaxation of replica scaling used in the design of the 1/40-scale model is acceptable for determining the first three launch-vehicle bending modes. The importance of proper representation of the tie-down condition and the importance of the inclusion of shear deformation are demonstrated.

INTRODUCTION

An important consideration in the design of launch vehicles is the dynamic response of these structures to input loads. The computation of these responses is facilitated by a knowledge of the normal modes of vibration. Thus, it is important to be able to obtain these modal data with confidence early in the launch-vehicle-development cycle. A convenient tool for this purpose is the structural model which may be used either to study full-scale response or to confirm the accuracy of calculated modal information. The use of structural models as opposed to full-scale test structures is attractive because of the great cost reduction in their construction and the reduced effort and manpower required to obtain experimental data. One modeling technique, referred to as replica modeling in

this report, in which the main load-carrying members are geometrically scaled reproductions of the full-scale members has been investigated with a 1/5-scale replica model of the Saturn I launch vehicle and with a 1/10-scale replica model of the Apollo-Saturn V launch vehicle. (See refs. 1 and 2, respectively.) Results presented in reference 3 indicate that the reliability of predicting full-scale vibration characteristics with replica models is good.

An important step in the development of a structural model is the selection of a convenient scale factor. On one hand, it is desirable that the model be small because of the ease and economy with which experimental data can be obtained with a small model; on the other hand, practical considerations such as maintaining tolerance requirements and the manufacture of thin-gage materials impose limitations on the amount of size reduction possible in a replica model.

The concept of a dynamically similar model may be used to achieve further size reduction than that which is possible with a replica model. The full-scale stiffness and mass distributions are scaled but less detail is achieved in the model than exists in either the full-scale launch vehicle or its replica model. Thus, a departure from replica reproduction is introduced with the assumption that this departure does not affect the overall response characteristics as compared with scaled full-scale characteristics. Therefore, a 1/40-scale dynamically similar model of the Apollo-Saturn V launch vehicle has been constructed as a part of a launch-vehicle model program at the Langley Research Center. The vibration characteristics of this model have been investigated in order to obtain information concerning the degree of relaxation from replica scaling which can be employed successfully to predict overall vibration characteristics.

The purpose of this report, therefore, is to present the lateral vibration characteristics of the 1/40-scale dynamically similar model of the Apollo-Saturn V launch vehicle as determined by analysis and experiment. A preliminary indication of the validity of using small dynamically similar models is given by a comparison of data presented here with preliminary data from the 1/10-scale replica model of the Apollo-Saturn V launch vehicle.

SYMBOLS

A cross-sectional area of beam element

C_1, C_2, C_3, C_4 influence coefficients defined by equations (4) to (7)

E Young's modulus of elasticity

F shaker force

f	frequency
G	shear modulus of elasticity
g	damping factor
h	total deflection
I	moment of inertia of cross section
K	Timoshenko shear constant
ℓ	length of beam element
M	bending moment
m	mass
n	number of cycles
P	transfer matrix for a mass element
r	mean radius of vehicle shell wall
s	percent difference, $\frac{f_a - f_e}{f_e} \times 100$
T	transfer matrix for beam element
$\tilde{T}$	transfer matrix relating state vector at initial end to that at final end
$\overline{T}$	transfer matrix after application of boundary conditions
V	transverse shear
x	coordinate along length of beam element
y_o	initial vibration amplitude
y_n	vibration amplitude after n cycles

Z	state vector
$\overline{Z}$	state vector after application of boundary condition
φ	slope of bending curve
ν	Poisson's ratio
ω	natural circular frequency

Subscripts:

a	analytical
e	experimental
i	ith mass or beam element
L	left
R	right
o	initial
n	number of cycles
t	tip

MODEL DESCRIPTION

The 1/40-scale model is dynamically similar to the Apollo-Saturn V launch vehicle and consists of simulated S-IC, S-II, and S-IVB stages, Apollo payload, and launch escape system. The complete model is shown in figure 1, supported by a 2-cable suspension system designed to provide the proper simulation for free-free lateral vibration response studies. A sketch showing some of the model details, station numbers, and definition of the model components is presented in figure 2(a). A detailed description of the model is given in reference 4.

The model is 279.4 cm long with a maximum tank diameter of 25.17 cm. When fully ballasted with propellant simulation weights, the model mass is 148.03 kg. This

mass corresponds to a full-scale weight condition in which the first stage is 85 percent full and all upper stages are 100 percent full. As indicated in reference 4, space limitations preclude modeling of the lift-off condition with this model.

The skin-stringer cylindrical sections were designed on the basis of scaled AE distributions with the skin thickness and stringer dimensions chosen so that an equivalent EI was attained. The number of stringers used on the model was reduced to 40 from the 168 and 204 used on the full-scale oxidizer and fuel tanks, respectively. The bulkhead thicknesses were also determined on the basis of a scaled AE distribution. The scaling of the AE distributions account for differences in material between model and full-scale vehicle as discussed in reference 4. The bending stiffness of the model, which was obtained by direct scaling from the full-scale stiffness, is presented in figure 3. The shear stiffness shown in figure 4 was computed from the bending stiffness by use of the relation

$$KAG = \frac{KEI}{r^2(1 + \nu)} \tag{1}$$

with the shear coefficient K taken as 1/2 and Poisson's ratio ν taken as 1/4. The model mass distribution is given in figure 5.

In the S-II and S-IVB stages, the propellant weight is simulated by cylindrical ballast weights attached to the model skin. This system of ballast weights was used in the upper stages because in all configurations considered, these stages are either 100 percent full or empty. When empty, no propellant mass is considered and when 100 percent full it is assumed that there is no sloshing and thus the propellant can be treated as a rigidly attached mass. In the S-IC stage there are, in addition to the ballast weights, two propellant slosh simulators attached to the model skin. These simulators are spring-mass devices based on a mathematical slosh analogy given in reference 5 and the full-scale slosh frequencies with the tanks 85 percent full. These simulators have a mass of 9.05 kg and a spring stiffness of 542.4 N/cm for an uncoupled frequency of 12.3 Hz. The position of attachment of the simulators for different propellant levels is shown in figure 2(b).

Sketches of the simulated F-1 and J-2 engines, with the associated mass and stiffness, are given in figure 6. The section of the engine shown crosshatched in figure 6 gives the proper stiffness and the remainder of the engine is designed to give proper inertial properties. There are five F-1 engines located on the S-IC stage, four located symmetrically at the outside, and one at the center supported by a cross beam of an I-configuration. Five J-2 engines are located on the S-II stage, supported by a truncated cone whose small end contains a cross beam. The simulated engines are mounted on the

base of this cone in the same arrangement as the engines on the S-IC stage. The S-IVB stage has a single J-2 engine, also mounted on a thrust cone.

The simulation of the lunar module was achieved with a rigid mass attached to the lunar module adaptor. The dimensions of this mass are such as to give the proper weight, center of gravity, and moment of inertia.

TEST PROGRAM

Three test configurations, configuration I denoting the complete vehicle, configuration II denoting the S-II and S-IVB stages with the Apollo payload, and configuration III denoting the S-IVB stage with the Apollo payload, were investigated with simulated free-free boundary conditions. Only configuration I was investigated with a simulated cantilevered boundary condition. Each configuration was studied with various weight conditions corresponding to different flight times. A summary of the test configurations investigated, both experimentally and analytically, is given in table I.

Suspension and Shaker System

Free-free boundary conditions for the model were simulated with the use of a two-cable suspension system supporting the model as shown in figure 1. The holddown posts of the model were attached to a cruciform cradle from which the model was supported by two vertical cables. Tipover stability of the model was provided by a restraining cable located at the top of the S-IVB stage as illustrated in figure 1. The restraining force was varied by varying the distance between the cables at the top supports. The characteristics of this suspension system are discussed in detail in reference 6. One electromagnetic shaker having a capacity of 45 N was used for all the tests performed. The shaker was supported by cables and was oriented to apply the force at the cradle (station 5.08 cm) normal to the plane of the vertical suspension cables.

The 1/40-scale Saturn V model was mounted on a test stand, as shown in figure 7, to simulate a cantilever test condition. The test stand used was an aluminum cylinder 14 cm high with a 24.4-cm outside diameter and a 2.04-cm wall thickness. The model was bolted to the test stand through its tiedown posts. The shaker was attached to the S-II thrust structure (model station 106.5 cm) and was supported by two cables, a support setup similar to the setup used during the free-free tests.

Instrumentation

Vibration response, frequency, and damping of the model were determined from the output of lightweight crystal-type accelerometers. An effort to measure the center-line motion of the model (beam-type motion) was made by measuring the response at the

various flanged joints of the model where possible local response effects were minimized. Accelerometer locations are shown in figure 2(a).

The data were recorded on analog tape and were digitized by means of a 24-point-per-cycle conversion. The digitized data were then reduced by means of a harmonic analysis to determine the model deformations from which the fundamental component of the response was converted to normalized mode shapes.

Laboratory Procedure

A frequency sweep with constant shaker force input was performed over the frequency range of 10 Hz to 300 Hz for each test condition of the model. The principal bending modes were detected by monitoring the acceleration level measured at the tip of the model. Each resonance was then tuned to its maximum response where the resonant frequency, mode shape, and damping of the elastic bending modes were determined. The damping was obtained by cutting the input signal to the shaker at the resonant frequency and recording the output of accelerometers on oscillographs. The amplitudes were read from oscillographs and plotted on semilogarithmic paper with a straight line faired through the points. The damping factor g was obtained from the relation:

$$g = \frac{1}{n\pi} \log_e \frac{y_o}{y_n}$$

where

y_o initial vibration amplitude

y_n vibration amplitude after n cycles

ANALYSIS

In this section the idealization of the model used in the analysis and the method of analysis and solution are discussed. As discussed previously, configuration I is used to denote the complete vehicle, whereas configuration II denotes the S-II and the S-IVB stages with the Apollo payload. The presence of the launch escape system is indicated in the specification of the particular condition under consideration. The S-IVB stage with the Apollo payload is referred to as configuration III. A summary of the configurations and weight conditions analyzed is given in table I.

Physical Idealization

For the purpose of analysis, the model was treated as a beam (fig. 2(b)) and the engines on the S-IC, S-II, and S-IVB stages, and the slosh mass simulators were treated as branch beams. A lumped-mass finite elastic element idealization was used. The

effect of shear deformation was included but that of rotary inertia was neglected. In the idealization of configuration I, 55 massless beams connecting 56 masses were used to represent the main beam. This arrangement, in general, resulted in beam elements 5.08 cm long with exceptions occurring at the branch locations. For the staged configurations, a beam element length of 2.54 cm was used, the total number of elements depending on the configuration. The minimum number of elements used was 36 for configuration III.

The engine branches were idealized as multi-degree-of-freedom beams as shown in figure 6. On both the S-IC and S-II stages there is a cluster of five engines. Each engine in a cluster was idealized as shown in figure 6 and these representations were then combined into a single branch having equal impedance. On all three stages the engine thrust structure was considered to be rigid.

The fuel-slosh simulators were idealized as single-degree-of-freedom branches. The location of these branches on the main beam was varied to correspond to different first-stage propellant levels. These locations are given in figure 2(b).

The structure that simulates the lunar module, although attached to the main structure as a branch, was treated as a rigidly attached mass as were the nonsloshing-propellant-simulation ballast weights. The tiedown structure of the model used in the cantilever configuration (see fig. 7) was idealized as translational and rotational springs connecting the vehicle to the ground as indicated in figure 8.

Method of Analysis and Solution

The analysis was performed by use of the state-vector transfer-matrix technique. (See ref. 7.) This method is based on relating the state vector on one side of an element, whether it is a mass or elastic element, to the state vector on the other side. For a beam element, the state vector Z consists of shear, moment, rotation, and deflection. With the sign convention shown in sketch (a), the transfer relation for a mass element without rotary inertia is

$$\begin{Bmatrix} V \\ M \\ \varphi \\ h \end{Bmatrix}_{L_i} = \begin{bmatrix} 1 & 0 & 0 & \omega^2 m_i \\ 0 & 1 & 0 & 0 \\ 0 & 0 & 1 & 0 \\ 0 & 0 & 0 & 1 \end{bmatrix} \begin{Bmatrix} V \\ M \\ \varphi \\ h \end{Bmatrix}_{R_i} \tag{2}$$

where L_i denotes the left side of the ith mass; R_i, the right side; and m_i, the ith mass. For an elastic beam element with sign convention shown in sketch (a), the transfer relationship is

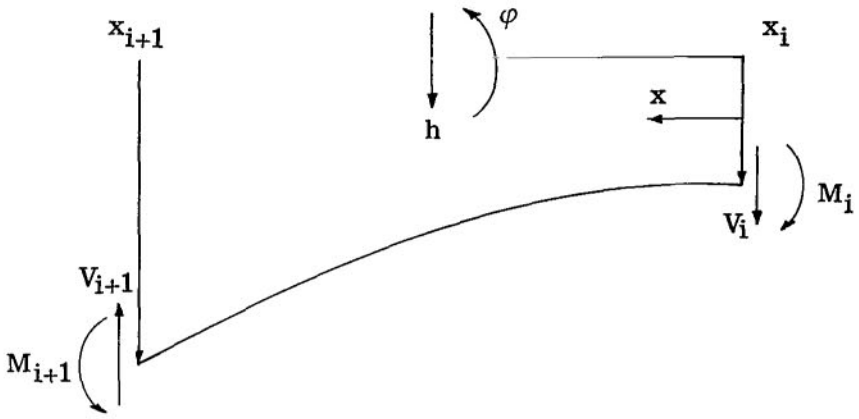

Sketch (a)

$$\begin{Bmatrix} V \\ M \\ \varphi \\ h \end{Bmatrix}_{i+1} = \begin{bmatrix} 1 & 0 & 0 & 0 \\ \ell & 1 & 0 & 0 \\ C_1 & C_2 & 1 & 0 \\ C_3 & C_4 & \ell & 1 \end{bmatrix}_i \begin{Bmatrix} V \\ M \\ \varphi \\ h \end{Bmatrix}_i \tag{3}$$

where ℓ is the length of the beam connecting the ith and i + 1th mass. The influence coefficients C_1, C_2, C_3, and C_4 for this element are given by

$$C_1 = \int_{x_i}^{x_{i+1}} \frac{x}{EI(x)}\, dx \tag{4}$$

$$C_2 = \int_{x_i}^{x_{i+1}} \frac{1}{EI(x)}\, dx \tag{5}$$

$$C_3 = \int_{x_i}^{x_{i+1}} \frac{(\ell - x)x}{EI(x)} - \frac{1}{KAG(x)}\, dx \tag{6}$$

$$C_4 = \int_{x_i}^{x_{i+1}} \frac{l - x}{EI(x)}\, dx \tag{7}$$

and can be derived by using the theorems of the slope deviation method; however, they differ from those given in reference 7 in that these constants have the advantage of not requiring that the stiffness be constant over the length of the beam element used. The use of these constants removes the necessity of assuming average values of bending and shear stiffness over the length of an element for cases with complicated stiffness distributions. The influence coefficients for this analysis were computed from the bending and shear stiffness distributions in figures 3 and 4, respectively, by use of a standard numerical integration routine.

In addition to the transfer matrices for elastic beam and mass elements, a transfer matrix for crossing the juncture of a branch with the main beam is required. To obtain this relation, the joint shown in sketch (b) is considered.

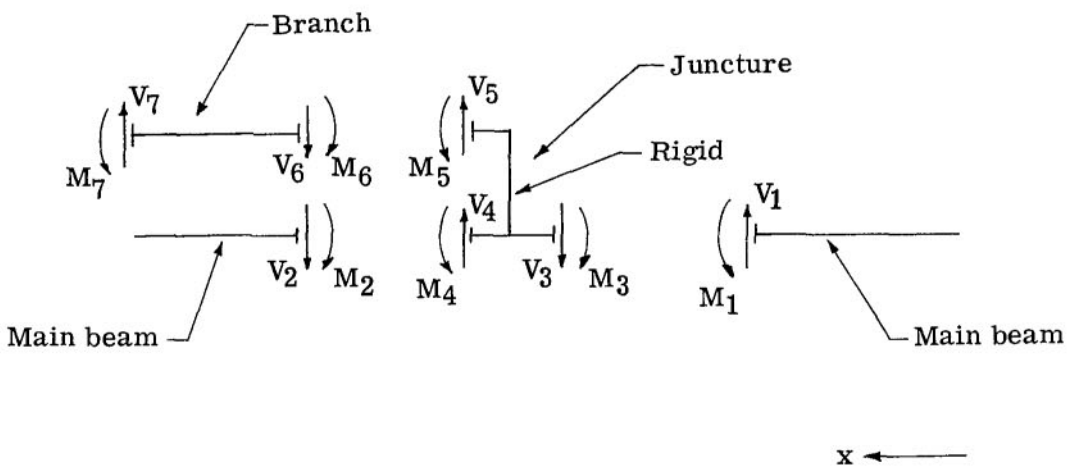

Sketch (b)

Continuity requires that

$$\left.\begin{aligned} h_6 = h_5 = h_4 = h_3 = h_2 = h_1 \\ \varphi_6 = \varphi_5 = \varphi_4 = \varphi_3 = \varphi_2 = \varphi_1 \end{aligned}\right\} \tag{8}$$

and equilibrium requires that

$$\left.\begin{aligned} V_5 + V_4 &= V_3 \\ M_5 + M_4 &= M_3 \\ V_1 &= V_3 \\ M_1 &= M_3 \\ V_5 &= V_6 \\ M_5 &= M_6 \\ V_2 &= V_4 \\ M_2 &= M_4 \end{aligned}\right\} \tag{9}$$

A relation between z_1 and z_2 is desired; thus, for equilibrium

$$\begin{Bmatrix} V_2 \\ M_2 \end{Bmatrix} = \begin{Bmatrix} V_1 \\ M_1 \end{Bmatrix} - \begin{Bmatrix} V_6 \\ M_6 \end{Bmatrix} \tag{10}$$

and for continuity

$$\begin{Bmatrix} \varphi_2 \\ h_2 \end{Bmatrix} = \begin{Bmatrix} \varphi_1 \\ h_1 \end{Bmatrix} \tag{11}$$

The following transfer relation is constructed for the branch:

$$\begin{Bmatrix} V_7 \\ M_7 \\ \varphi_7 \\ h_7 \end{Bmatrix} = \left[\begin{array}{c|c} [T_1] & [T_2] \\ \hline [T_3] & [T_4] \end{array}\right] \begin{Bmatrix} V_6 \\ M_6 \\ \varphi_6 \\ h_6 \end{Bmatrix} \tag{12}$$

Since open-ended branches are being considered, $V_7 = 0$ and $M_7 = 0$. Therefore,

$$\begin{Bmatrix} V_6 \\ M_6 \end{Bmatrix} = - [T_1]^{-1} [T_2] \begin{Bmatrix} \varphi_6 \\ h_6 \end{Bmatrix} \tag{13}$$

but by continuity

$$\begin{Bmatrix} \varphi_6 \\ h_6 \end{Bmatrix} = \begin{Bmatrix} \varphi_1 \\ h_1 \end{Bmatrix} \tag{14}$$

Therefore,

$$\begin{Bmatrix} V_2 \\ M_2 \\ \varphi_2 \\ h_2 \end{Bmatrix} = \left[\begin{array}{c|c} I & [T_1]^{-1}[T_2] \\ \hline O & [I] \end{array}\right] \begin{Bmatrix} V_1 \\ M_1 \\ \varphi_1 \\ h_1 \end{Bmatrix} \tag{15}$$

which is the relation needed for crossing the branch juncture on the main beam and is used in the same manner as the transfer matrices for the beam and mass element.

To determine the natural modes and frequencies, the transfer matrix for each of the elements, masses, and elastic beams are calculated to obtain relations (2) and (3). Then, by starting at the initial end of the beam, the first mass which is numbered zero can be written:

$$Z_{L,o} = P_o Z_{R,o} \tag{16}$$

where P_o is the transfer matrix for the mass as in equation (2). For the beam attached to this mass,

$$Z_1 = F_o Z_o \tag{17}$$

where F_o is the transfer matrix for the beam as in equation (3). But continuity and equilibrium require that

$$Z_{L,o} = Z_o \tag{18}$$

thus,

$$Z_1 = F_o P_o Z_{R,o} \tag{19}$$

A continuation of this process of applying continuity and equilibrium at joining members and using transfer matrices across members results in

$$Z_i = F_{i-1} P_{i-1} \cdots F_o P_o Z_{R,o} \tag{20}$$

When a branch juncture is encountered, a transfer matrix as in equation (15) is generated and used in equation (20) in the same manner as the transfer matrices for mass and beam elements. The state vector at the initial end of the beam is related to that at the final end by

$$Z_{L,f} = \tilde{T} Z_{R,o} \tag{21}$$

The matrix T in equation (21) is a function of frequency. By applying two homogeneous boundary conditions to each end of the beam, equation (21) becomes

$$0 = \overline{T}\, \overline{Z}_{R,o} \tag{22}$$

where $\overline{T}$ is a matrix of order 2 and $\overline{Z}_{R,o}$ consists of the unspecified elements of the state vector at the initial end of the beam. If $\overline{Z}_{R,o}$ is to exist, then

$$\text{Det } \overline{T} = 0 \tag{23}$$

which is the frequency equation. On the digital computer, this equation is solved by determinant plotting in the following manner: the matrix equation (21) and determinant $\overline{T}$ are computed for incremental values of frequency and any changes in the sign of determinant $\overline{T}$ indicates a zero crossing. At each zero crossing, an increasingly smaller increment of frequency is used to compute determinant $\overline{T}$ until it is within a specified tolerance. This procedure gives the natural frequency and thus in equation (22) one of the elements is chosen and the others are found relative to it. With $\overline{Z}_{R,o}$ known, $Z_{R,o}$ is known, and Z_i can be calculated for all stations by using equation (20) to provide the modal displacements, slopes, moments, and shears.

To provide for the connection of a mass to the ground by a translational and/or rotational spring, the transfer matrix (2) is replaced by the following matrix:

$$\begin{Bmatrix} V \\ M \\ \varphi \\ h \end{Bmatrix}_{L_i} = \begin{bmatrix} 1 & 0 & 0 & m\omega^2 - K_h \\ 0 & 1 & K_\varphi & 0 \\ 0 & 0 & 1 & 0 \\ 0 & 0 & 0 & 1 \end{bmatrix} \begin{Bmatrix} V \\ M \\ \varphi \\ h \end{Bmatrix}_{R_i} \tag{24}$$

where K_h is the translational spring and K_φ is the rotational spring.

RESULTS AND DISCUSSION

The natural modes and frequencies of the 1/40-scale dynamic model of the Apollo-Saturn V launch vehicle as determined from analysis and experiment are presented in tables II to IV and in figures 9 to 20. The modes presented are those corresponding to overall response of the model. A summary of the natural frequencies and modal damping for configuration I with free-free boundary conditions is given in table II.

The mode shapes for configuration I with free-free boundary condition are shown in figures 9 to 12. With the S-IC stage empty and the upper stages 100 percent full, the first three modes show predominant model bending motion whereas the fourth and fifth modes show predominant engine motion. For the remaining three weight conditions of configuration I, with free-free boundary conditions, the first mode found in the analysis is a mode in which the motion of the slosh mass simulator predominates and the model undergoes rigid body motion. Experimentally, this slosh mass simulator mode was found to have measurable response at station 264 only for the 15-percent weight condition. Therefore, a mode shape is presented only for this weight condition. The experimental frequencies given in figures 11(a) and 12(a) for the slosh mass simulator mode for the 50-percent and 85-percent weight condition were obtained by monitoring the response of the slosh mass simulator. Examination of figures 10(a), 11(a), and 12(a) indicates that the ratio of the response at station 264 to the responses of the lower slosh mass predicted by the analysis decreases with increasing fuel level; thus, both analysis and experiment show that the motion of the model in the slosh mode decreases with increasing fuel level. In the remaining modes for the 15-percent, 50-percent, and 85-percent weight conditions, bending motion of the model predominates. The modal damping for all fuel levels is found to be small but there is a general trend of increased damping for higher mode number.

Examination of the experimental free-free mode shapes for the 15-percent, 50-percent, and 85-percent weight conditions shows that there is very little motion of the

lunar module relative to the main vehicle structure, and thus validates the analytical assumption that the lunar module could be treated as a rigidly attached mass.

The natural frequencies for the vehicle in the cantilever configuration are summarized in table III and the mode shapes are plotted in figures 13 and 14. With the vehicle empty, four beam bending modes were obtained, the fourth mode shown in figure 13(d) being accompanied by large engine motions. With the S-IC 85 percent full and all upper stages 100 percent full, a mode shown in figure 14(b) in which motion of the fuel-slosh-simulation mass predominates was found along with five beam bending modes. In the tests of the cantilever configuration, the branch motions were not monitored and thus are not shown. To represent the cantilever attachment analytically, the mass located at the tiedown position was connected to the ground by translational and rotational springs to represent the tiedown structure. This arrangement is shown schematically in figure 8. The magnitudes of these springs were determined empirically by adjusting their magnitude until agreement between analysis and experiment was obtained for the first mode with the S-IC stage 85 percent full and all other stages 100 percent full. The magnitudes of these spring restraints which were used for both weight conditions investigated for the cantilever configuration are given in figure 8. The effect of the holddown representation on the frequencies is shown in table IV where the analytical frequencies with spring restraints and with cantilever boundary conditions are tabulated. It can be seen that an error as large as 32 percent can be introduced by improper representation of the holddown. Modal damping for the cantilevered vehicle is given in table III and is found to be small. The trend of increased damping with mode number is found for the empty vehicle but not for the full vehicle.

The measured and calculated natural frequencies for the staged configurations are summarized in table V and the natural mode shapes are shown in figures 15 to 19. It should be noted that for the staged configurations which have a lower length-diameter ratio, fewer modes with beam-type motion were found in the frequency range of the investigation. It was also found that the mode number in which engine motion predominates decreased as stages were removed. Both of these effects are especially noticeable when the launch escape system is removed.

The effect of including shear deformation in the analysis can be seen by comparing the frequencies given in table VI. The inclusion of shear deformation drops the difference between the analysis and experiment in the first mode from 8.1 percent to 2.3 percent. As expected, the effect becomes more pronounced for the higher modes.

In general, the agreement between analysis and experiment in both frequency and mode shape is considered to be good for the first two modes, the agreement being poorer in some of the higher modes.

The variation of the free-free bending frequencies with first-stage fuel level is shown in figure 20 for the analytical and experimental results presented in this report and for scaled experimental data from the 1/10-scale replica model of the Apollo-Saturn V. Examination of this figure shows that the experimental results of this investigation lie between the scaled 1/10-scale model experimental results and the 1/40-scale analytical results with good agreement for all fuel levels. The maximum deviations of the 1/40-scale model experimental data are 8.7 percent, 10.4 percent, and 8.6 percent in the first, second, and third modes, respectively, with respect to the scaled 1/10-scale model data. This result indicates that the degree of relaxation from replica scaling used in the design of the 1/40-scale dynamic model of the Apollo-Saturn V launch vehicle is acceptable with regard to determining the first three launch-vehicle bending modes.

CONCLUDING REMARKS

Analytically and experimentally determined lateral vibration characteristics for several configurations and weight conditions of the 1/40-scale dynamically similar model of the Apollo-Saturn V launch vehicle are presented as a part of the launch-vehicle dynamic-model program at the Langley Research Center. The results from both analysis and experiment show that the elastic modes are adequately characterized by beam bending-type motion. In the analysis the importance of shear deformation is demonstrated. In addition to the beam bending modes, modes in which the fuel-slosh simulator mass and engine motion predominate were observed experimentally and predicted analytically. In the frequency range investigated, fewer bending modes were observed for the staged configurations than for the complete vehicle.

The importance of proper representation of the tiedown structure for the cantilever configuration is demonstrated. A difference of 32 percent between the analytical and experimental first-mode frequency is obtained when an ideal cantilever was assumed in the analysis. To account for the flexibility of the tiedown structure, an empirical spring was introduced into the analysis to replace the ideal cantilever boundary condition.

A comparison of the results of this investigation with the scaled experimental results from the 1/10-scale model of the Apollo-Saturn V is made. This comparison indicates that the degree of relaxation from replica scaling used in the design of the 1/40-scale dynamic model of the Apollo-Saturn V launch vehicle is acceptable with regard to the determination of the first three launch-vehicle bending modes.

Langley Research Center,
National Aeronautics and Space Administration,
Langley Station, Hampton, Va., July 25, 1968,
124-08-05-18-23.

REFERENCES

1. Mixson, John S.; Catherines, John J.; and Arman, Ali: Investigation of the Lateral Vibration Characteristics of a 1/5-Scale Model of Saturn SA-I. NASA TN D-1593, 1963.

2. Leadbetter, S. A.; and Raney, J. P.: Model Studies of the Dynamics of Launch Vehicles. J. Spacecraft Rockets, vol. 3, no. 6, June 1966, pp. 936-938.

3. Mixson, John S.; and Catherines, John J.: Comparison of Experimental Vibration Characteristics Obtained From a 1/5-Scale Model and From a Full-Scale Saturn SA-1. NASA TN D-2215, 1964.

4. Catherines, John J.: Experimental Vibration Characteristics of a 1/40-Scale Dynamic Model of the Saturn V—Launch-Umbilical-Tower Configuration. NASA TN D-4870, 1968.

5. Bauer, Helmut F.: Fluid Oscillations in the Containers of a Space Vehicle and Their Influence Upon Stability. NASA TR R-187, 1964.

6. Herr, Robert W.; and Carden, Huey D.: Support Systems and Excitation Techniques for Dynamic Models of Space Vehicle Structures. Proceedings of Symposium on Aeroelastic Dynamic Modeling Technology, RTD-TDR-63-4197, pt. I, Aerospace Ind. Assoc., Mar. 1964, pp. 249-277.

7. Loewy, Robert G.; and Joglekar, Mukund M.: Matrix Holzer Analysis for Fully-Coupled Vibrations of Clustered Launch-Vehicle Configurations Including Applications to the Titan IIIC and Uncoupled Saturn I Cases. NASA CR-592, 1966.

TABLE I.- SUMMARY OF 1/40-SCALE MODEL CONFIGURATIONS AND WEIGHT CONDITIONS TESTED AND ANALYZED

Configuration I – complete vehicle
Configuration II without launch escape system – S-II, S-IVB stages with Apollo payload and launch escape system
Configuration II without launch escape system – S-II, S-IVB stages with Apollo payload;
Configuration III – S-IVB stage with the Apollo payload

Free-free				Cantilever
Configuration I	Configuration II with launch escape system	Configuration II without launch escape system	Configuration III	Configuration I
S-IC empty*	S-II 100% full*	S-II empty*	S-IVB empty	All tanks empty
S-IC 15% full*		S-II 100% full*	S-IVB 100% full	S-IC 85% full*
S-IC 50% full*				
S-IC 85% full*				

*All other tanks 100 percent full.

TABLE II.- COMPARISON OF ANALYTICAL AND EXPERIMENTAL FREQUENCIES AND EXPERIMENTAL DAMPING OBTAINED FOR CONFIGURATION I – FREE-FREE

Mode	Frequencies and damping for –											
	S-IC 85% full			S-IC 50% full			S-IC 15% full			S-IC empty		
	Analytical	Experimental		Analytical	Experimental		Analytical	Experimental		Analytical	Experimental	
	Frequency, Hz	Frequency, Hz	Damping, g	Frequency, Hz	Frequency, Hz	Damping, g	Frequency, Hz	Frequency, Hz	Damping, g	Frequency, Hz	Frequency, Hz	Damping, g
First bending	40.3	39.4	0.0079	42.1	40.6	0.0123	44.9	43.1	0.0107	45.3	43.8	0.0129
Second bending	77.7	71.7	.0108	84.9	78.6	.0318	92.4	85.5	.0173	93.1	85.8	.0162
Third bending	119.6	103.1	.0116	123.7	111.1	.0247	130.0	123.3	.0234	130.3	126.1	
Fourth bending	147.8	129.0	.0145	153.6	129.9	.0152						
Slosh	13.6	13.5		14.1	14.0		17.7	17.2	.0110			
S-IC engine				246.3			242.6			245.6	216.0	.0119
S-IVB engine	259.8			260.1			260.7			263.9	241.6	.0159
Suspension:												
(a) Rocking		.360			1.008			.360			.318	
(b) Pendulum		.307			.306							
(c) Rocking and pendulum								.288				

TABLE III.- SUMMARY OF FREQUENCY AND DAMPING RESULTS FOR CONFIGURATION I CANTILEVERED

Mode	Frequency and damping results for weight condition of –					
	No fuel			Complete fuel load		
	Analytical	Experimental		Analytical	Experimental	
	Frequency, Hz	Frequency, Hz	Damping, g	Frequency, Hz	Frequency, Hz	Damping, g
First bending	19.1	18.75	0.007	10.6	10.9	0.0163
Second bending	76.3	71.8	.0094	36.3	34.7	.0086
Third bending	122.6	118.6	.010	68.8	62.2	
Fourth bending	203.6	188.9	.0139	115.0	95.7	.0082
Fifth bending				141.6	127.0	
Slosh				13.3		
S-IC engine	241.8			242.6		
S-IVB engine	264.5			260.4		

TABLE IV.- COMPARISON OF FREQUENCIES FOR CONFIGURATION I

[First stage full showing the effect of boundary conditions]

Mode	Frequencies for boundary conditions of –		
	Cantilever, Hz	Spring restraint, Hz	Experimental, Hz
First	14.6	10.6	10.9
Second	39.7	36.3	34.7
Third	72.7	68.8	62.2
Fourth	117.0	115.0	95.7
Fifth	144.0	141.6	127.0

TABLE V.- SUMMARY OF FREQUENCY RESULTS FOR CONFIGURATIONS II AND III FREE-FREE

Mode	Frequency results for –									
	Configuration II; with launch escape system, all stages full		Configuration II; without launch escape system, all stages full		Configuration II; without launch escape system, S-II empty		Configuration III, S-IVB full		Configuration III, S-IVB empty	
	Analytical frequency, Hz	Experimental frequency, Hz	Analytical frequency, Hz	Experimental frequency, Hz	Analytical frequency, Hz	Experimental frequency, Hz	Analytical frequency, Hz	Experimental frequency, Hz	Analytical frequency, Hz	Experimental frequency, Hz
First bending	65.8	66.0	73.0	74.0	84.2	82.0	181.2	166.0	203.8	182.0
Second bending	124.8	123.0								
S-IVB engine	246.6	239.0	238.2		252.3					

TABLE VI.- THE EFFECTS OF SHEAR DEFORMATION OF THE FREE-FREE FREQUENCIES OF CONFIGURATION I

[First stage 85 percent full; all other stages 100 percent full]

Mode	Frequencies for –		
	Shear deformation, Hz	No shear deformation, Hz	Experimental, Hz
First bending	40.3	42.6	39.4
Second bending	77.7	85.4	71.7
Third bending	119.6	129.1	103.1

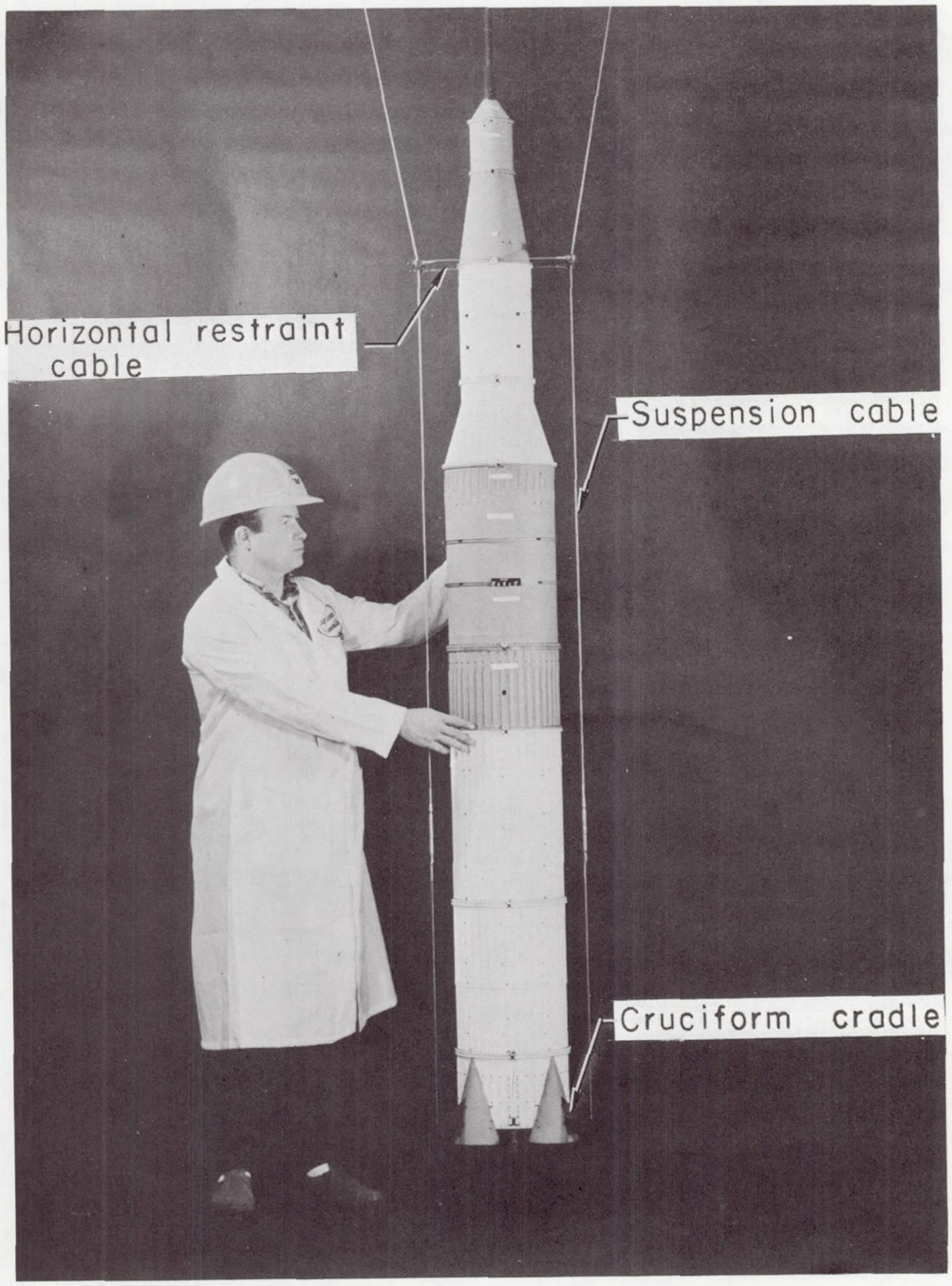

Figure 1.- 1/40-scale dynamic model of the Apollo-Saturn V launch vehicle. L-68-8501

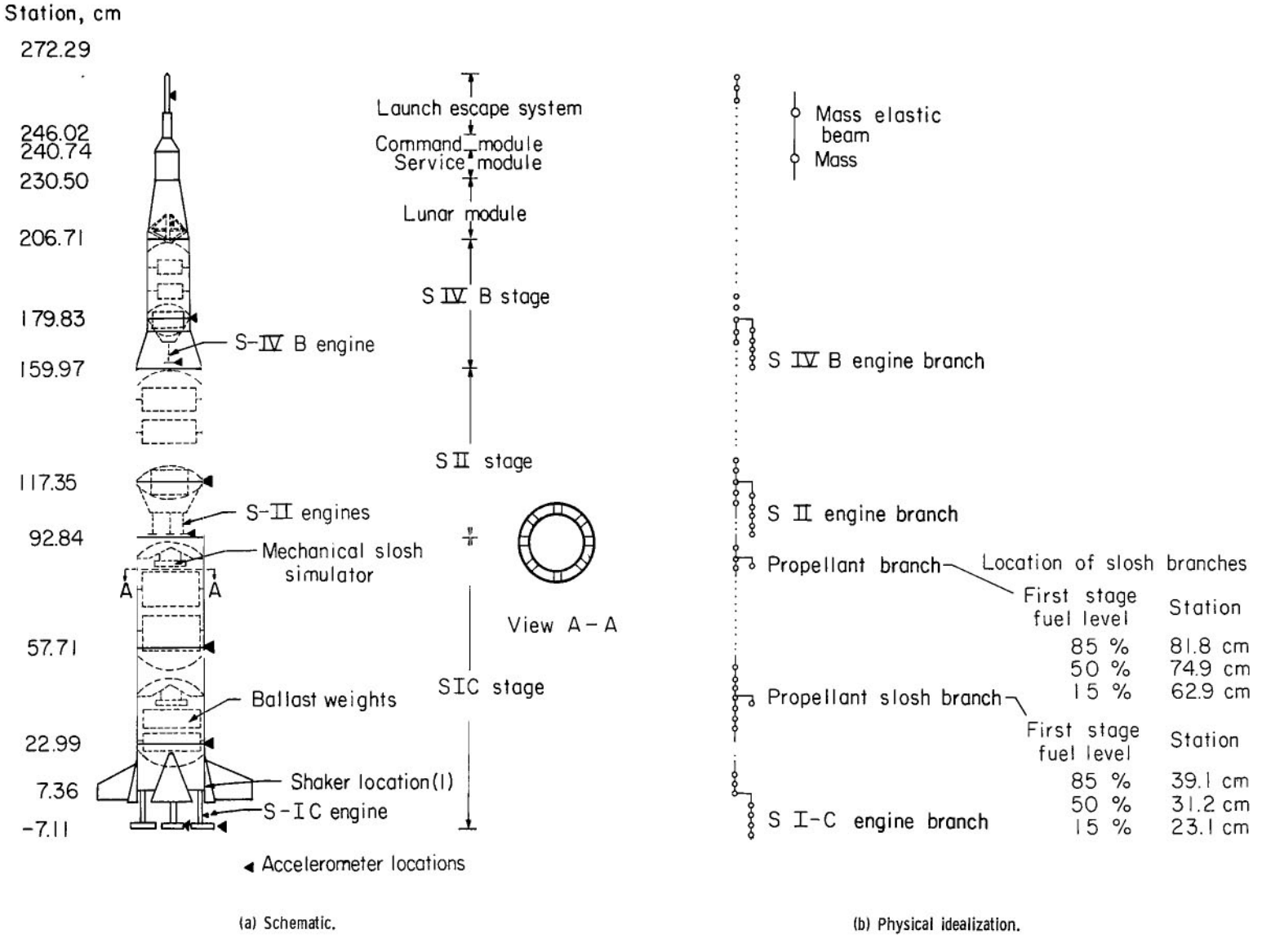

(a) Schematic.

(b) Physical idealization.

Figure 2.- Schematic drawing and physical idealization of the 1/40-scale dynamic model of the Saturn V launch vehicle.

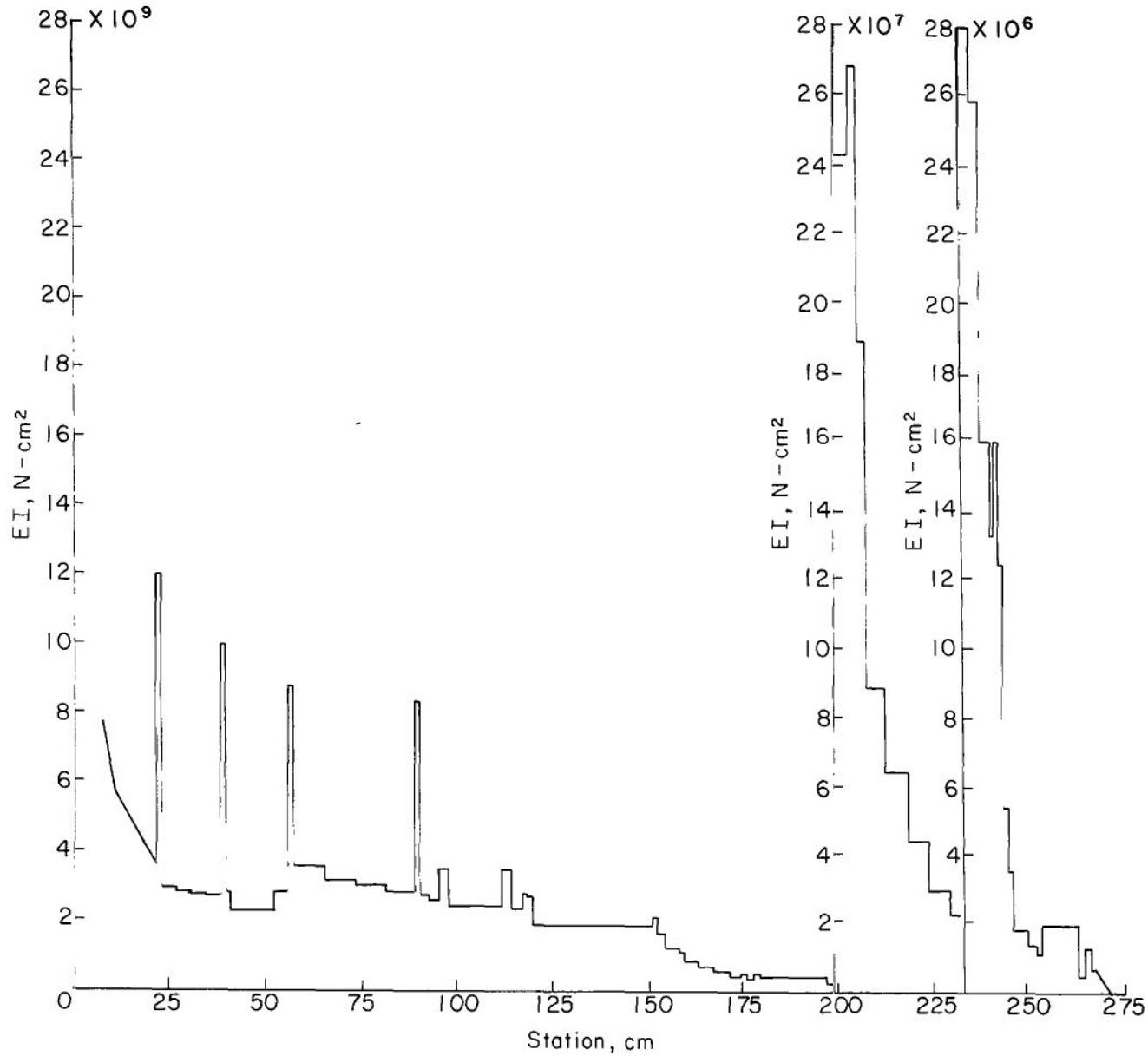

Figure 3.- Bending stiffness distribution of the 1/40-scale dynamic model of the Saturn V launch vehicle.

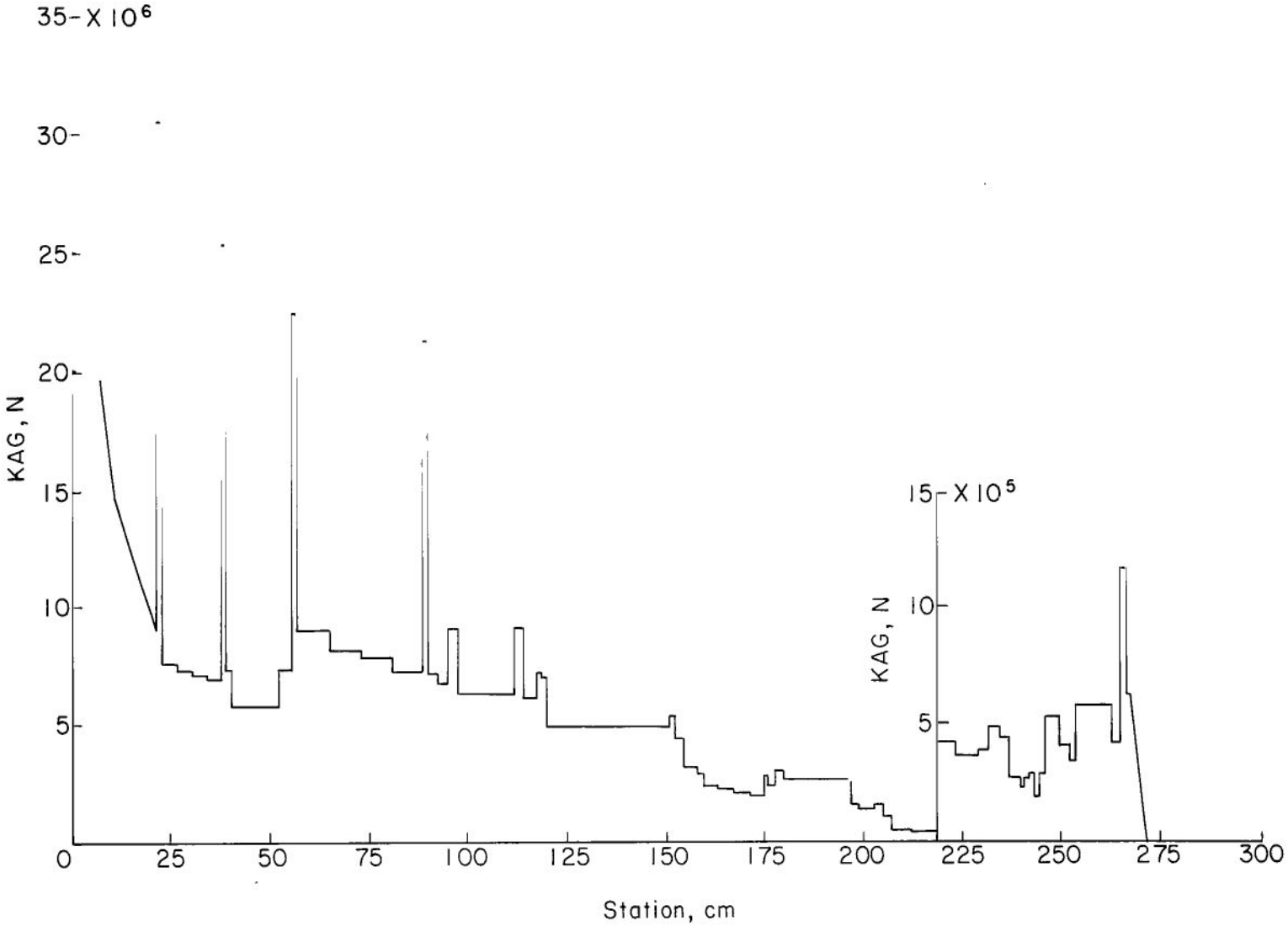

Figure 4.- Shear stiffness distribution of the 1/40-scale dynamic model of the Saturn V launch vehicle.

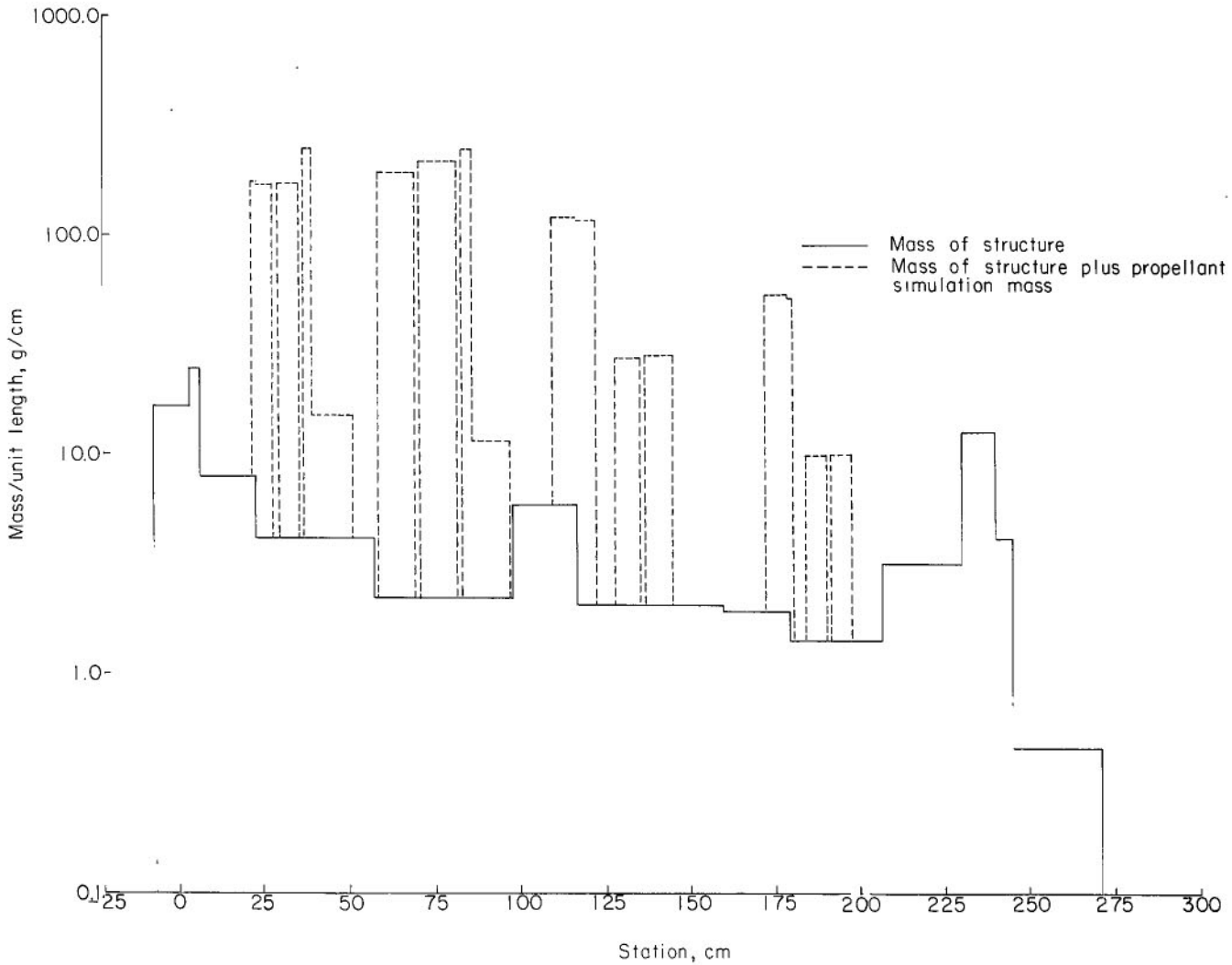

Figure 5.- Mass distribution of the 1/40-scale dynamic model of the Saturn V launch vehicle.

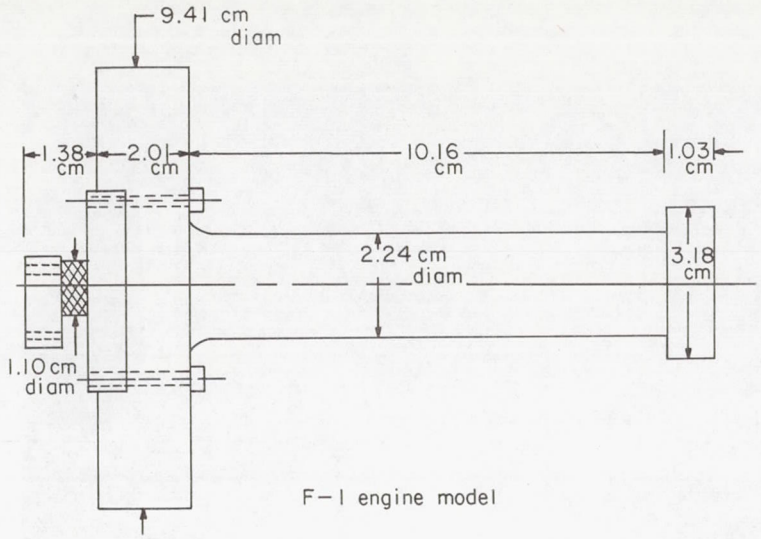

F-1 engine model

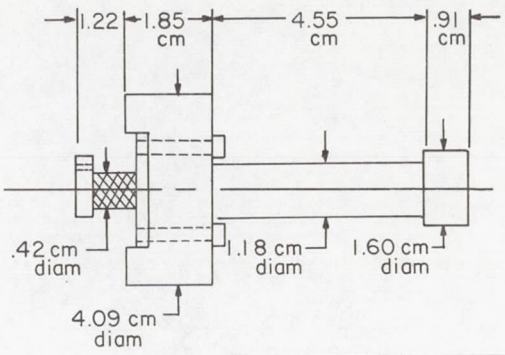

J-2 engine model

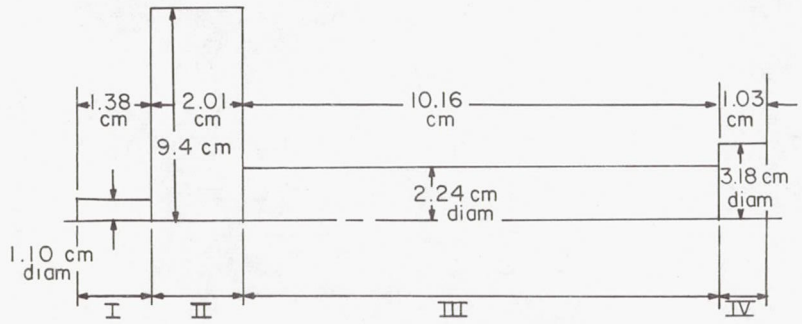

Idealization of F-1 engine model

Region	EI, (N-cm²)	Mass per unit length(g/cm)
I	5.094×10^5	0.2160
II	26.401×10^8	15.5960
III	8.678×10^6	.8900
IV	3.438×10^7	1.7760

(a) F-1 engine.

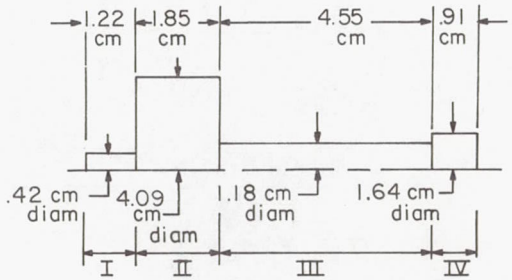

Idealization of J-2 engine model

Region	EI,(N-cm²)	Mass per unit length(g/cm)
I	3.042×10^4	0.0306
II	9.465×10^7	2.9900
III	6.486×10^5	.2450
IV	22.178×10^5	.4500

(b) J-2 engine.

Figure 6.- Idealization of engines.

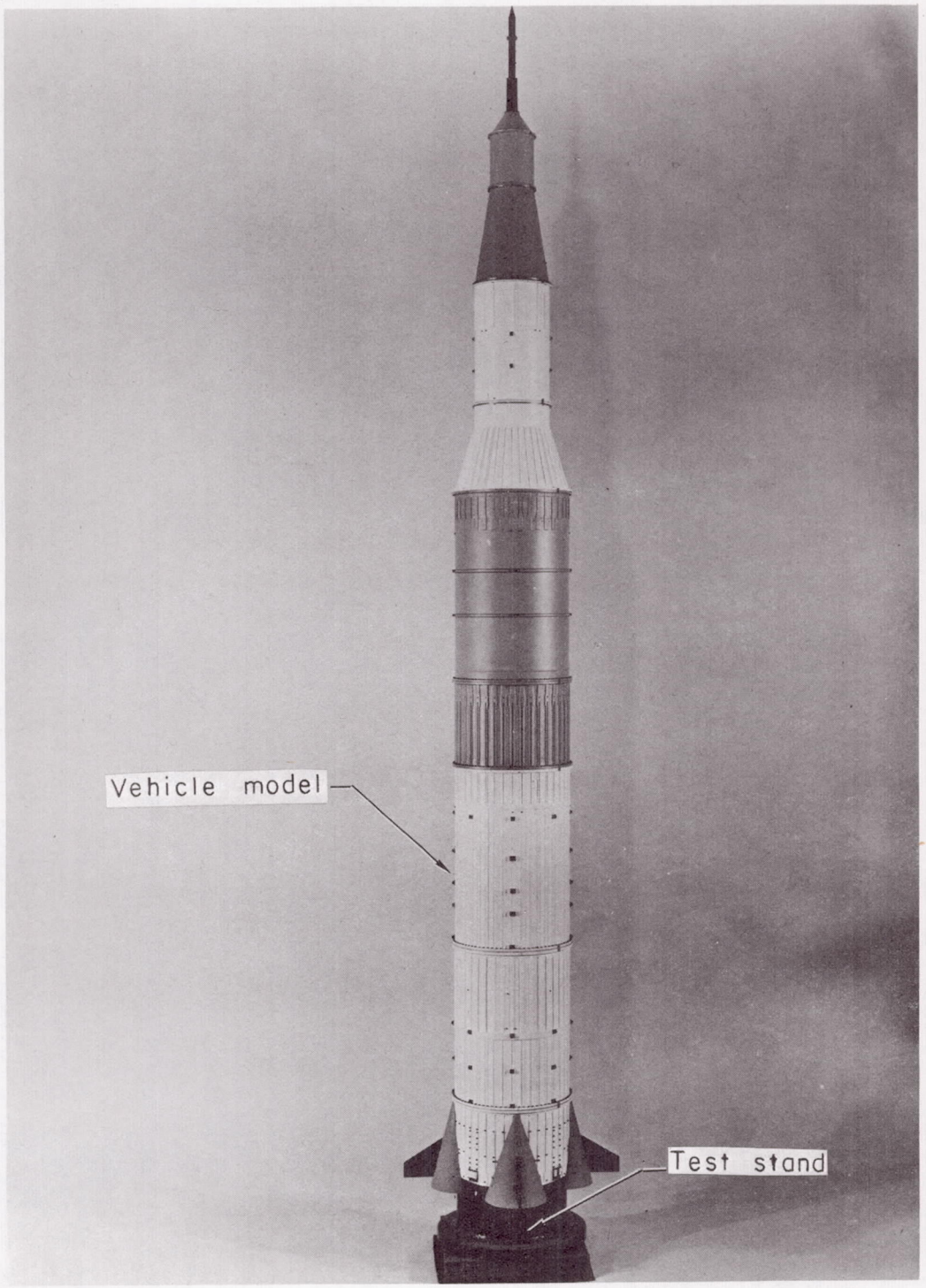

Figure 7.- 1/40-scale dynamic model of the Apollo-Saturn V launch vehicle on its cantilever test stand. L-68-8502

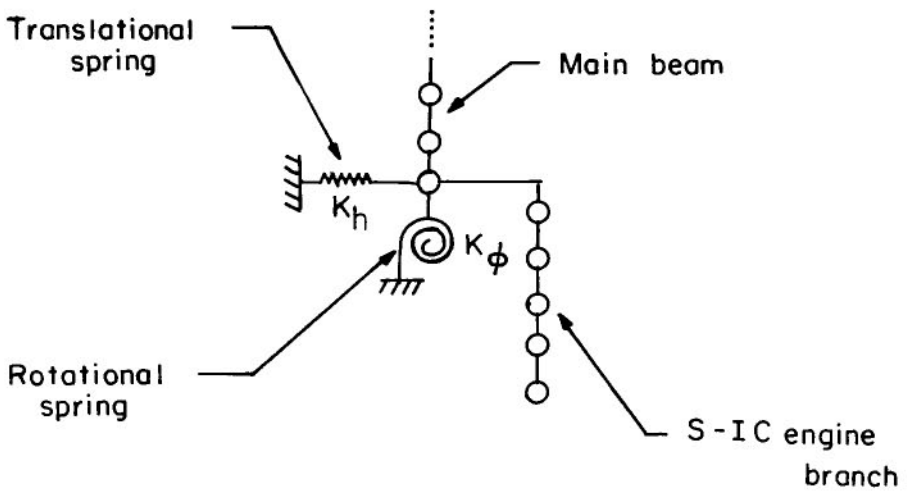

Figure 8.- Idealization of cantilever tiedown. $K_h = 1.715 \times 10^8$ N/cm; $K_\varphi = 1.421 \times 10^8$ N-cm/rad.

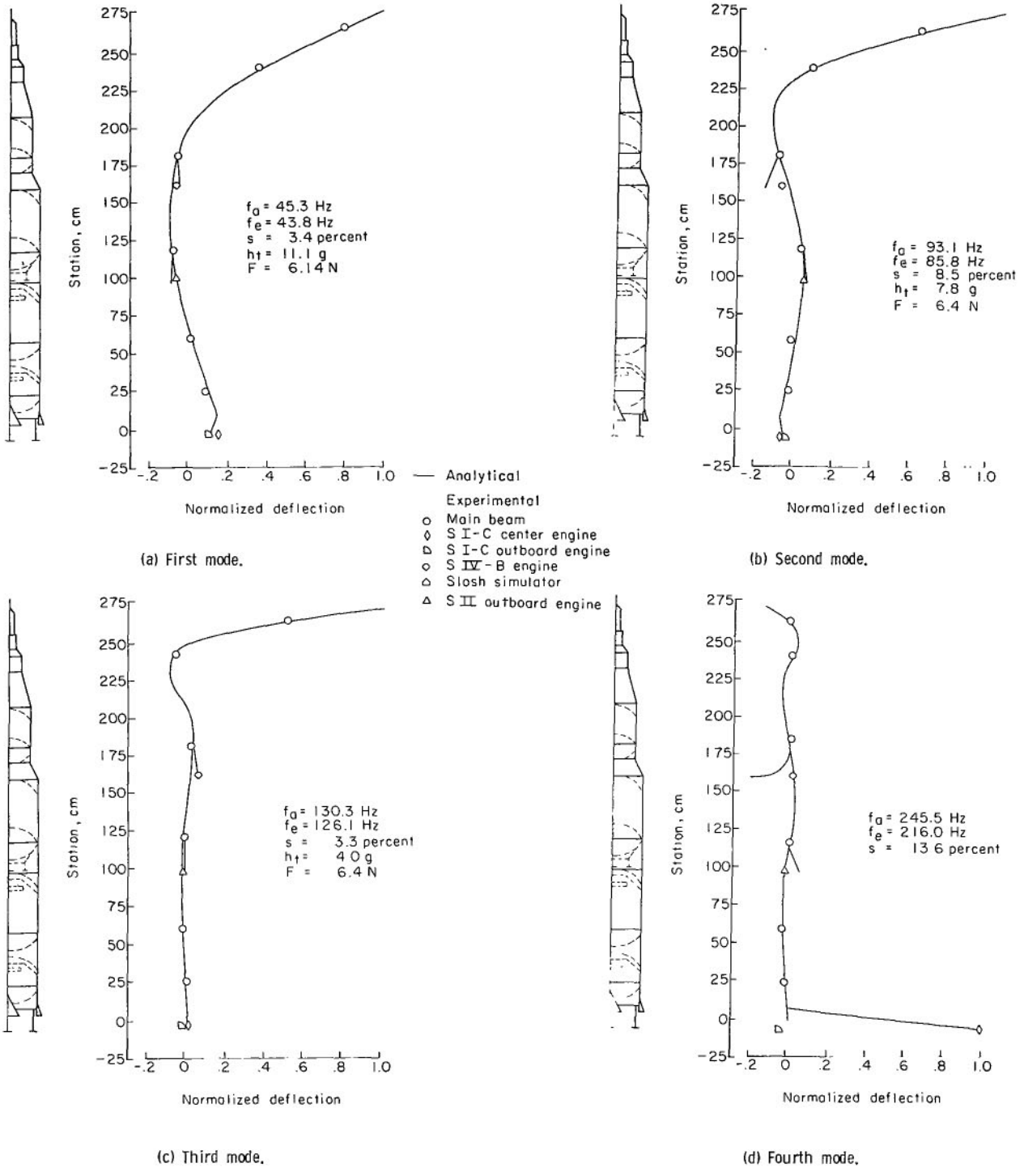

Figure 9.- Analytical and experimental free-free mode shapes for configuration I with the S-IC stage empty and all other stages 100 percent full.

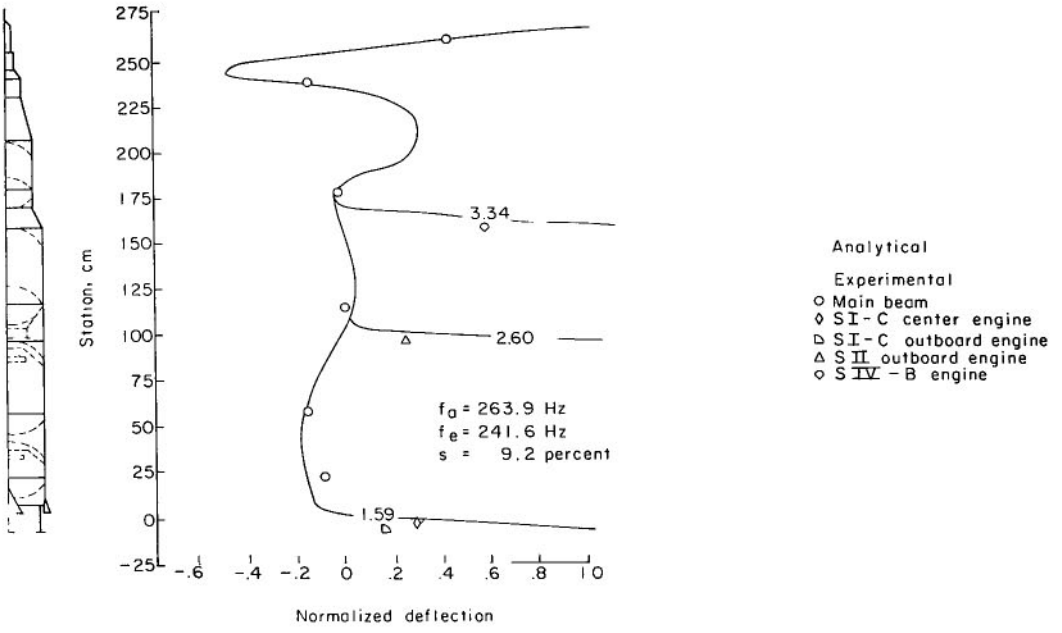

(e) Fifth mode.

Figure 9.- Concluded.

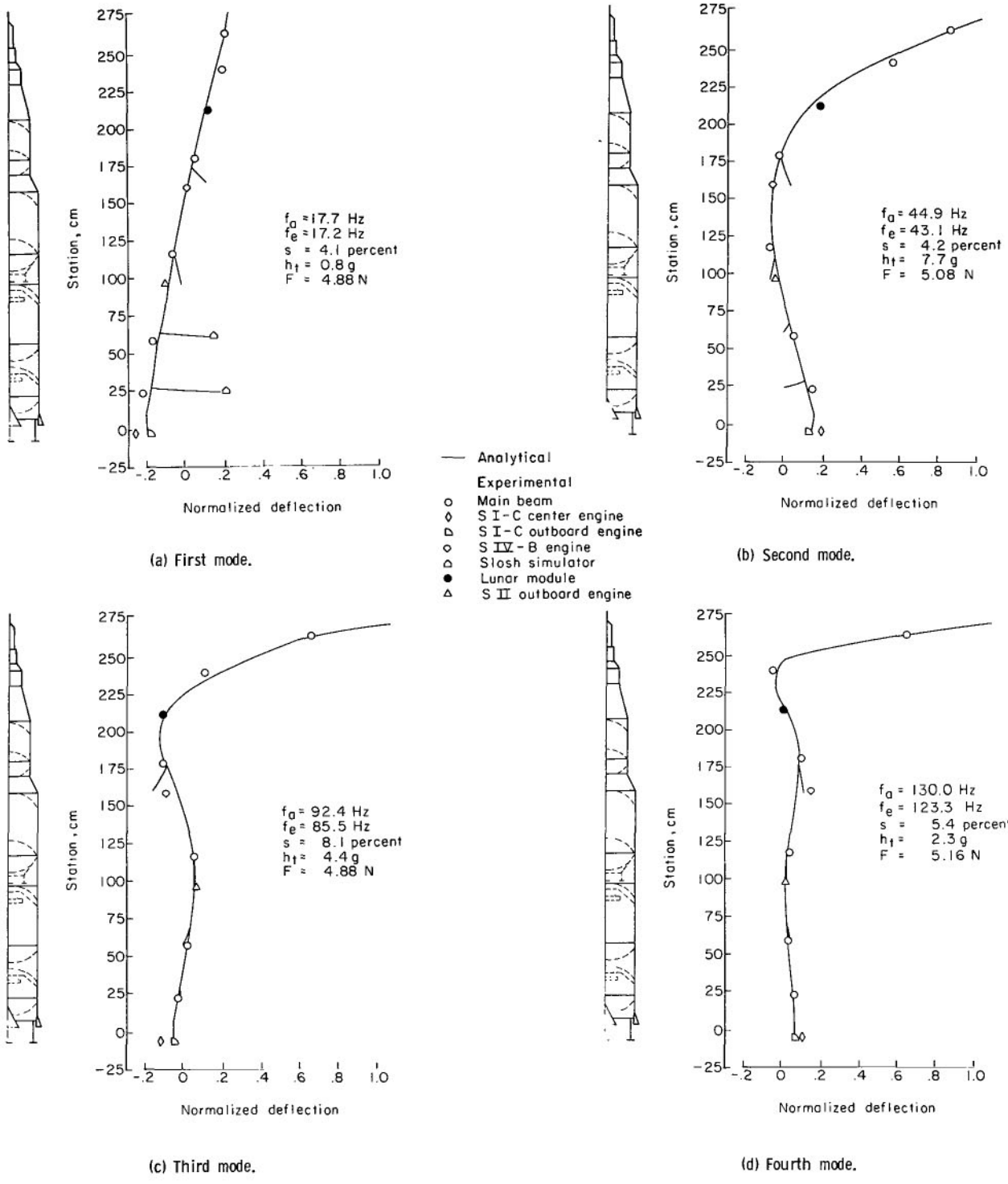

Figure 10.- Analytical and experimental free-free mode shapes for configuration I with the S-IC stage 15 percent full and all other stages 100 percent full.

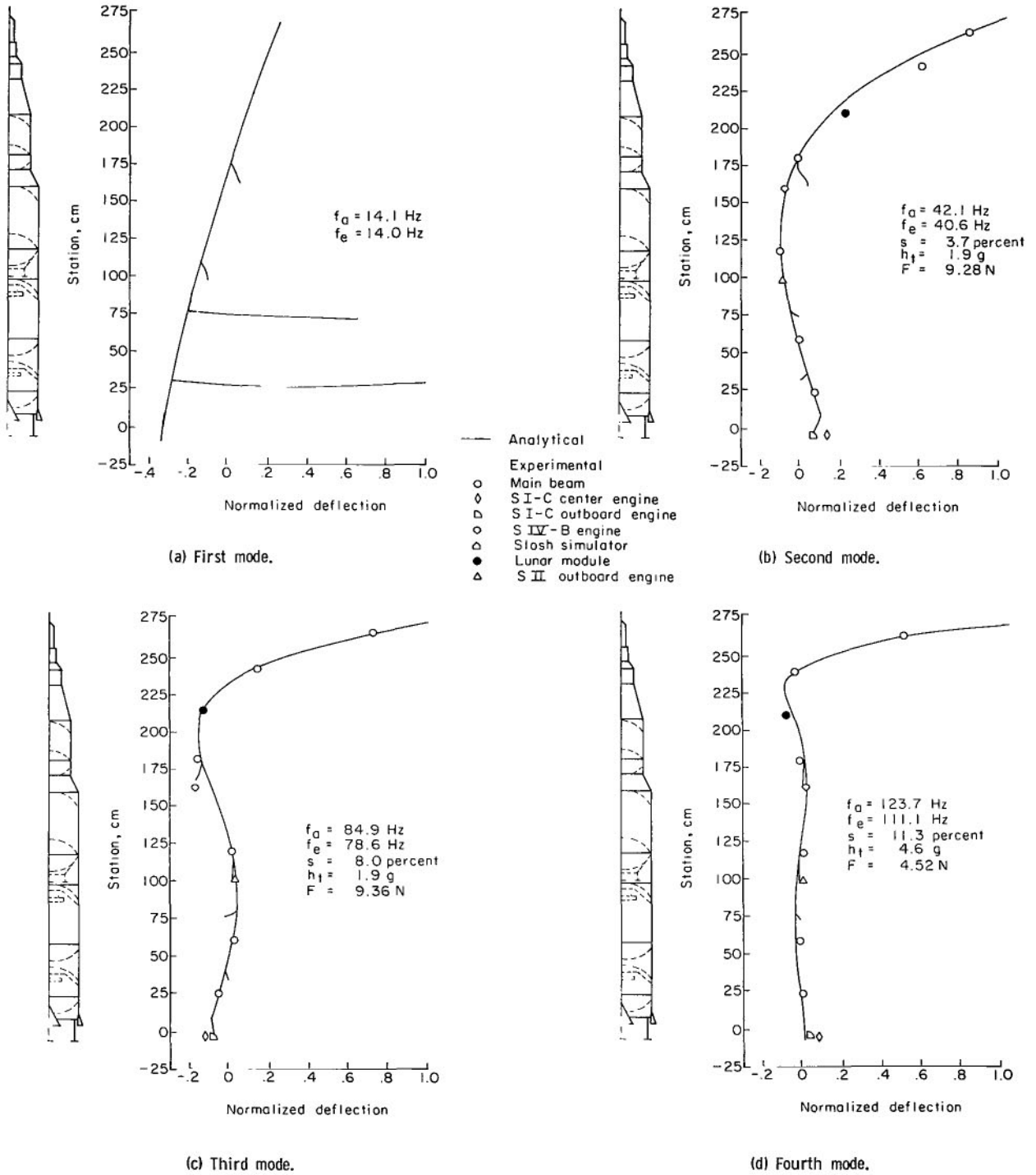

Figure 11.- Analytical and experimental free-free mode shapes for configuration I with the S-IC stage 50 percent full and all other stages 100 percent full.

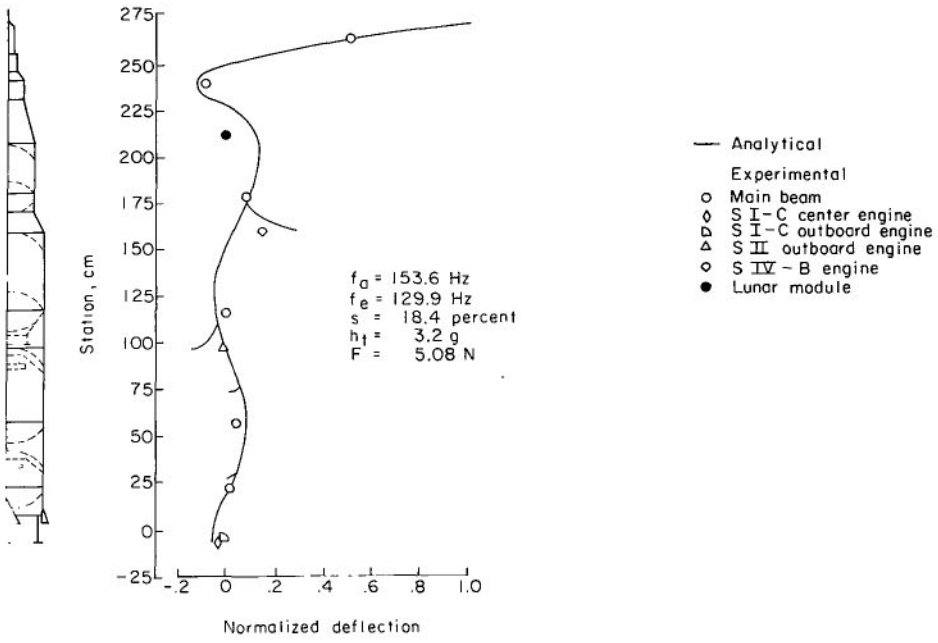

(e) Fifth mode.

Figure 11.- Concluded.

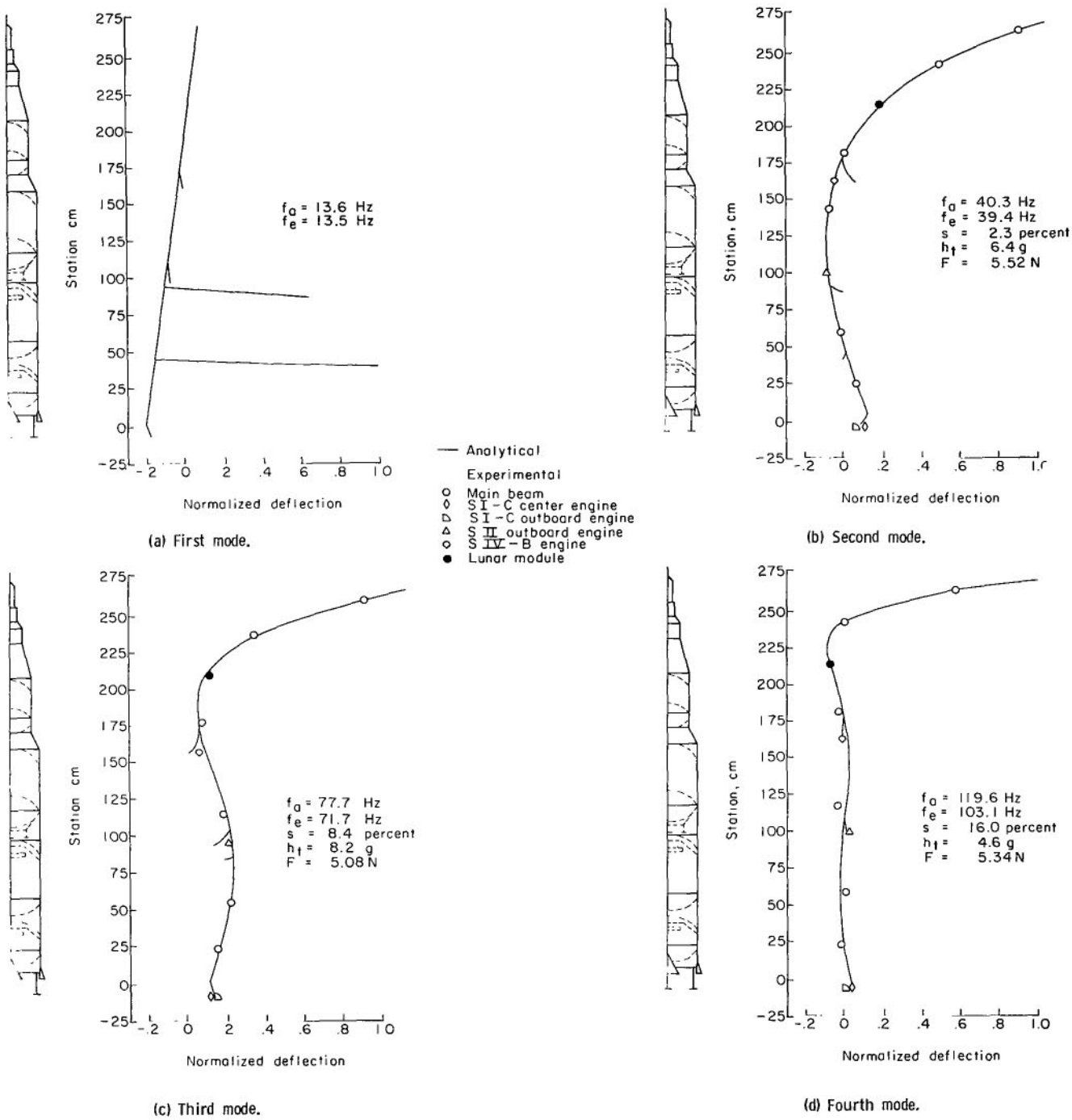

Figure 12.- Analytical and experimental free-free mode shapes for configuration I with the S-IC stage 85 percent full and all other stages 100 percent full.

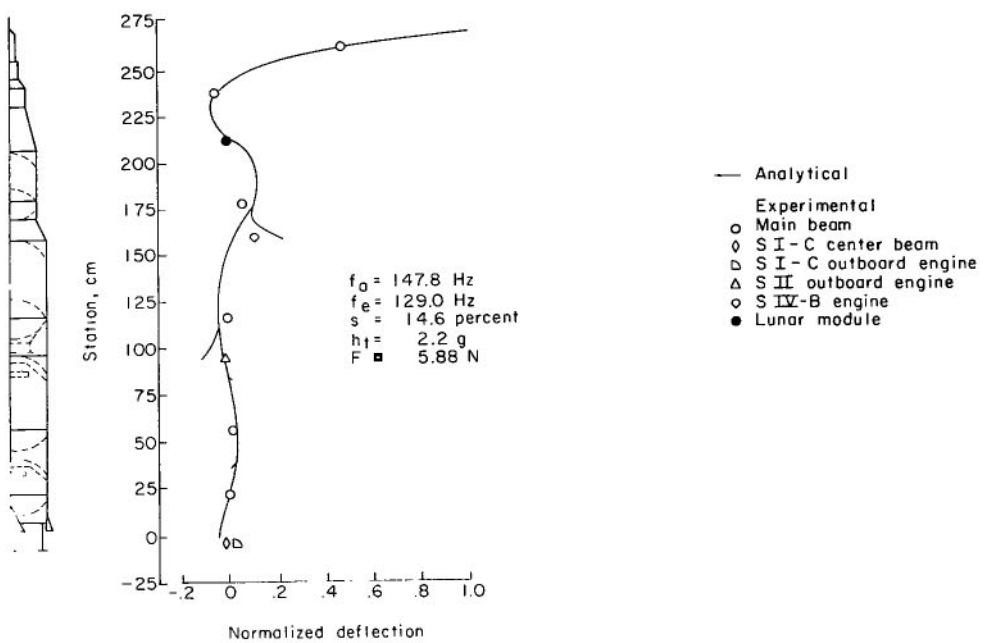

(e) Fifth mode.

Figure 12.- Concluded.

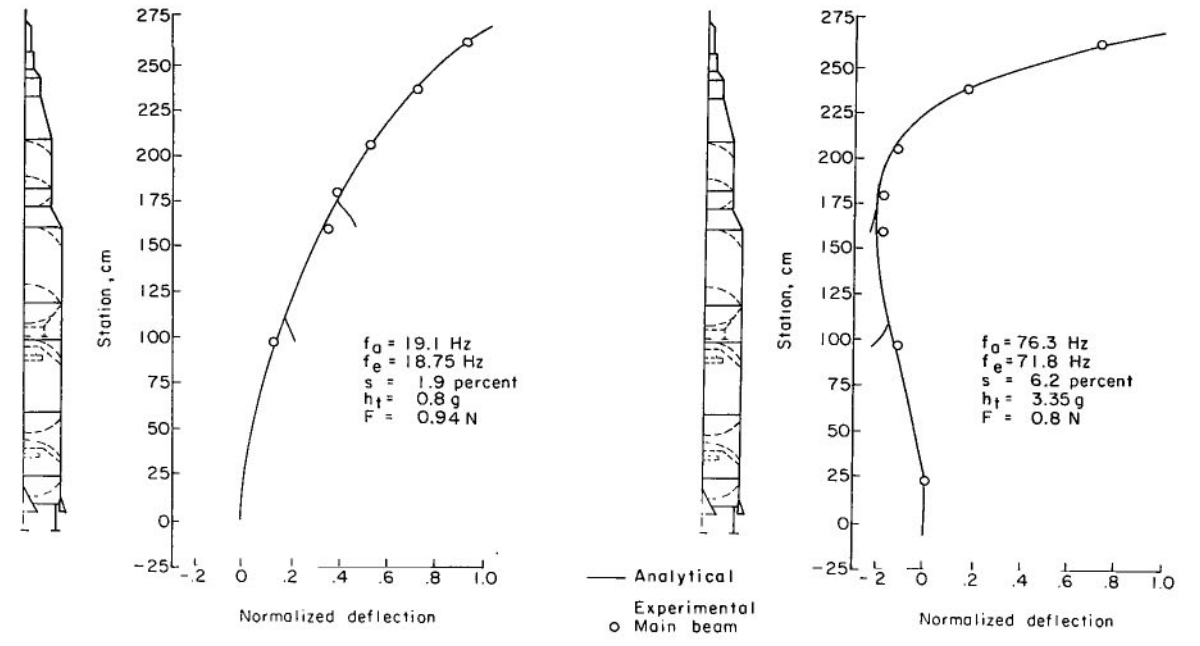

(a) First mode.

(b) Second mode.

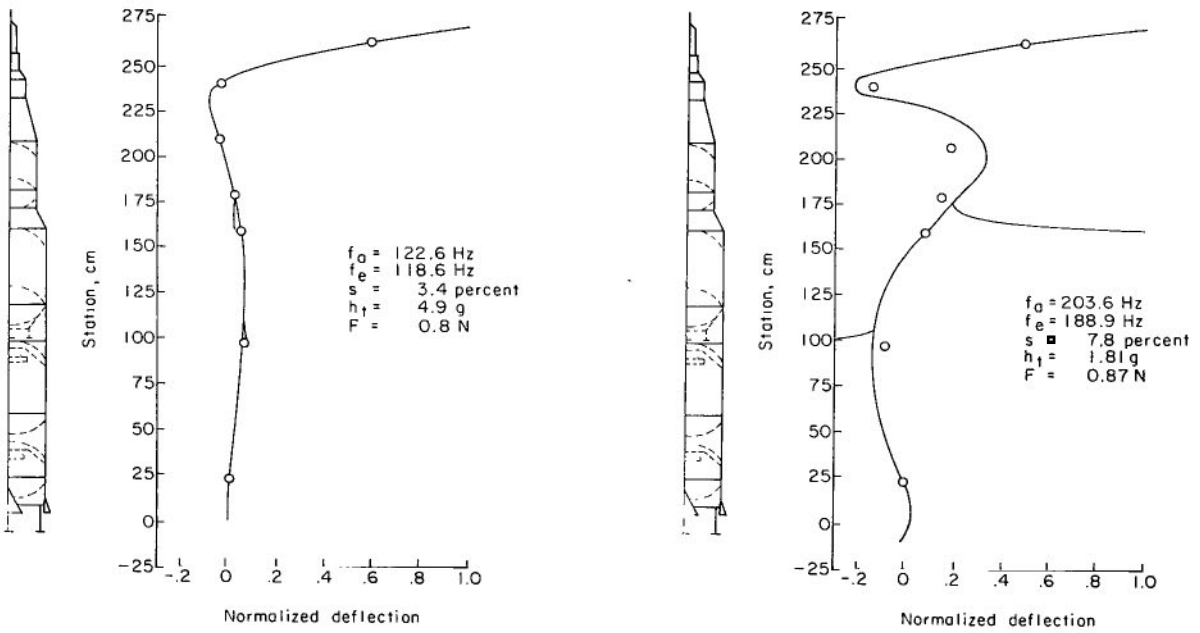

(c) Third mode.

(d) Fourth mode.

Figure 13.- Analytical and experimental cantilever mode shapes for configuration 1 with the vehicle empty and the Apollo full.

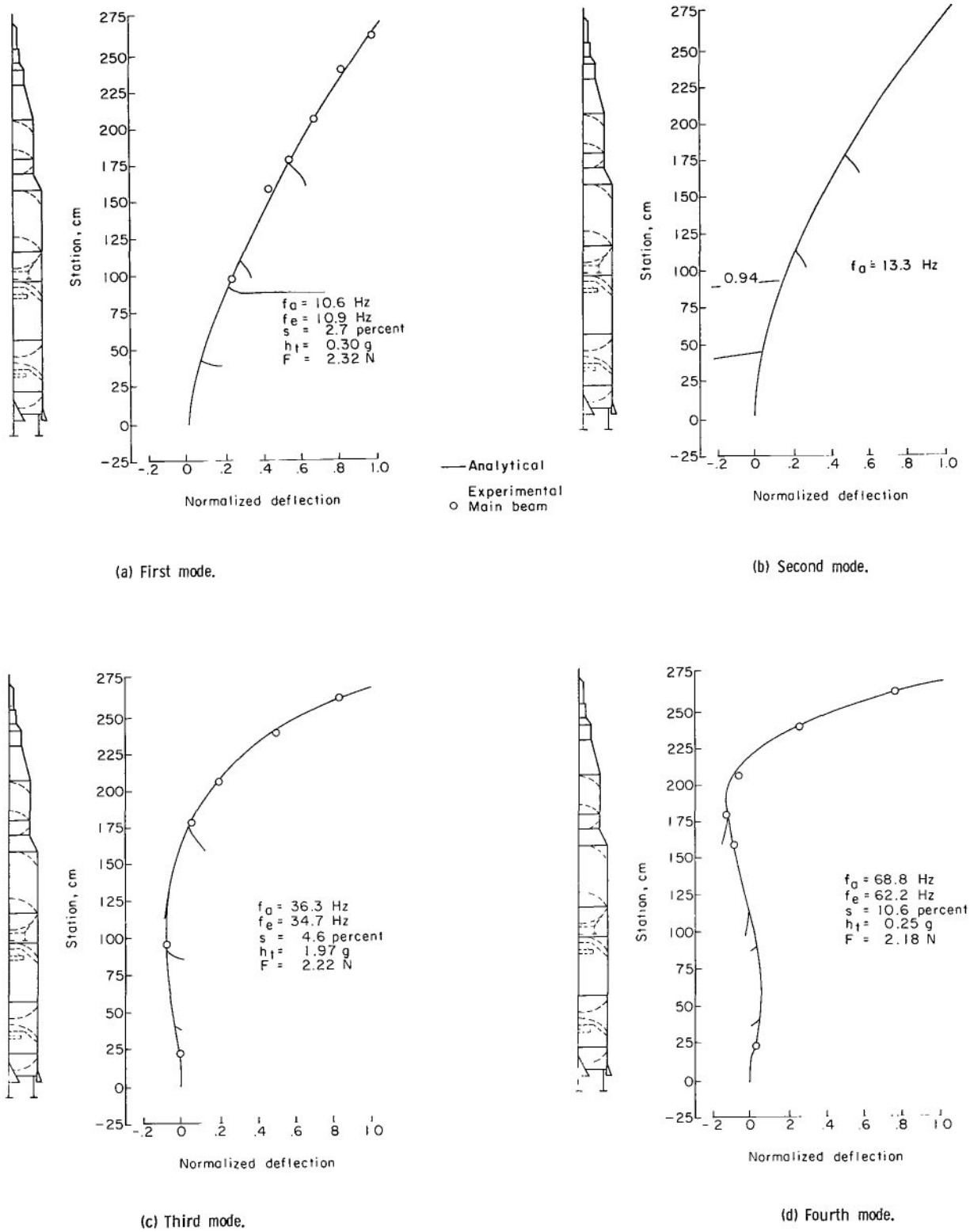

(a) First mode.

(b) Second mode.

(c) Third mode.

(d) Fourth mode.

Figure 14.- Analytical and experimental cantilever mode shapes for configuration I with the S-IC stage 85 percent full and all other stages 100 percent full.

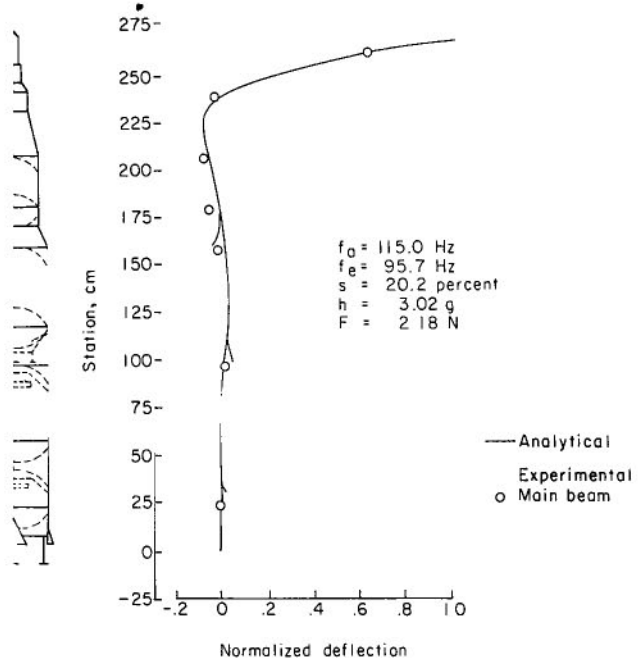

(e) Fifth mode.

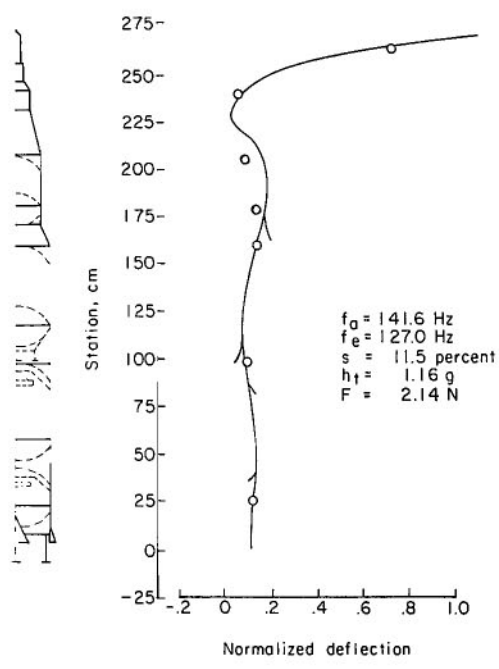

(f) Sixth mode.

Figure 14.- Concluded.

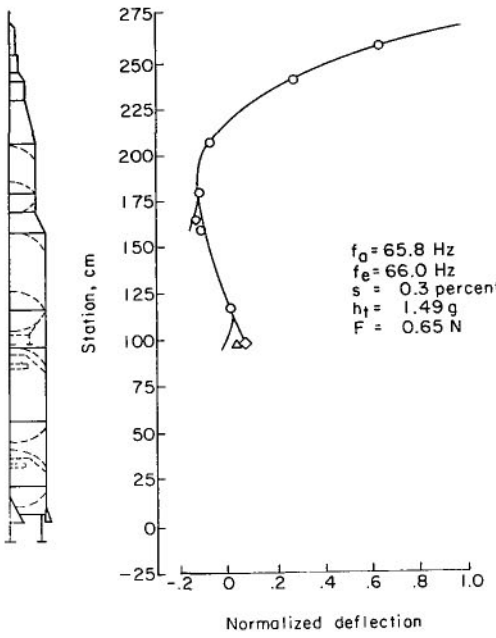

(a) First mode.

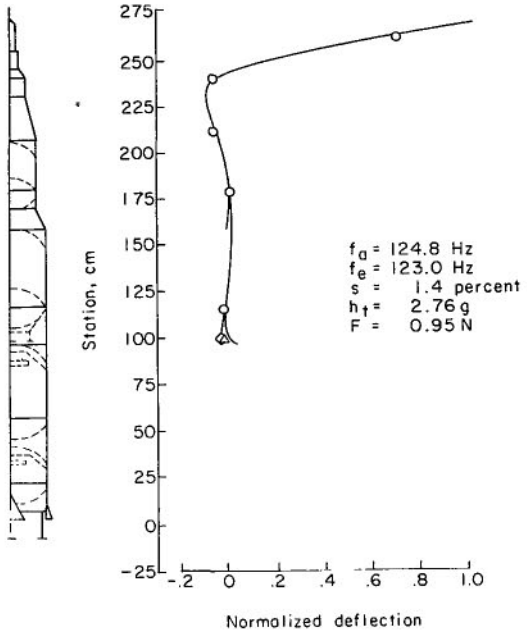

(b) Second mode.

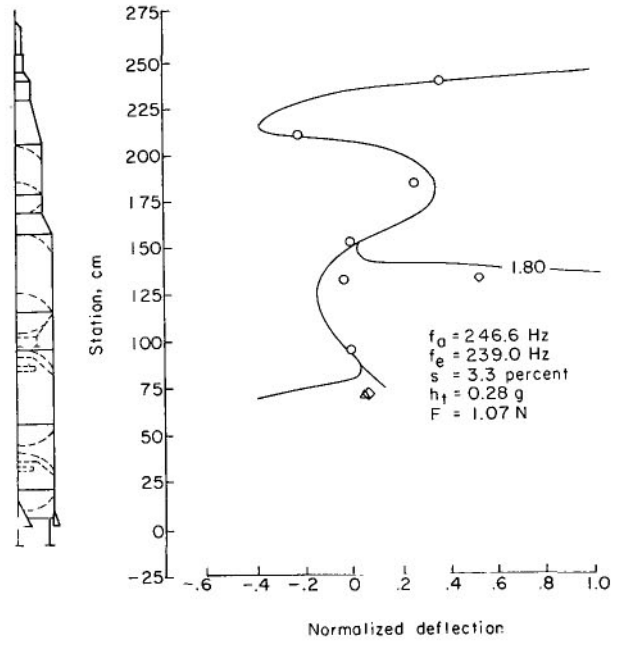

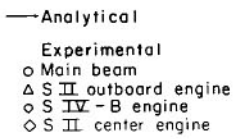

(c) Third mode.

Figure 15.- Analytical and experimental free-free mode shapes for configuration II with launch escape system. S-II, S-IVB, and Apollo stages 100 percent full.

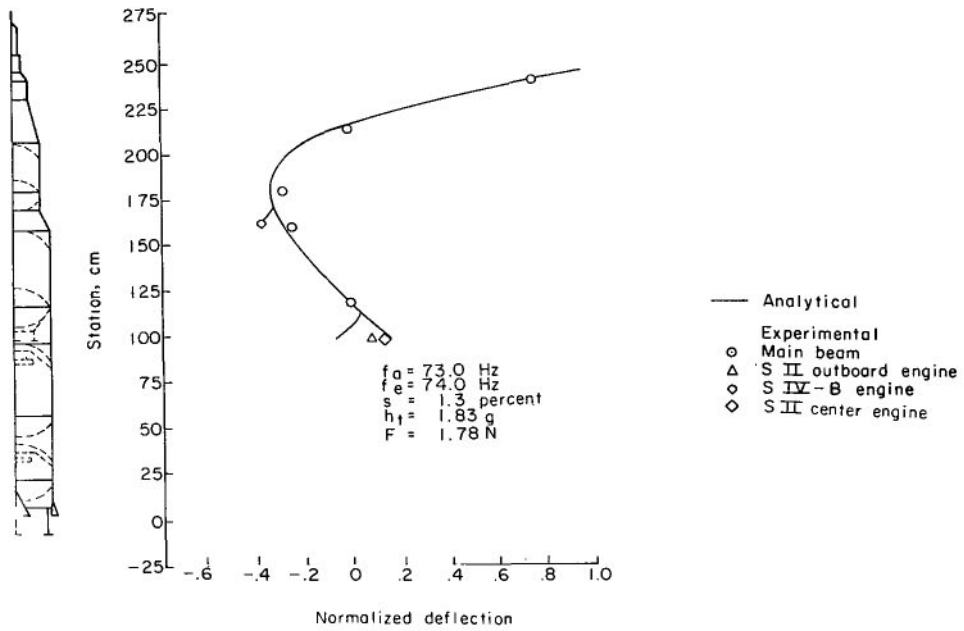

Figure 16.- Analytical and experimental free-free mode shape for configuration II without launch escape system. S-II, S-IVB, and Apollo 100 percent full.

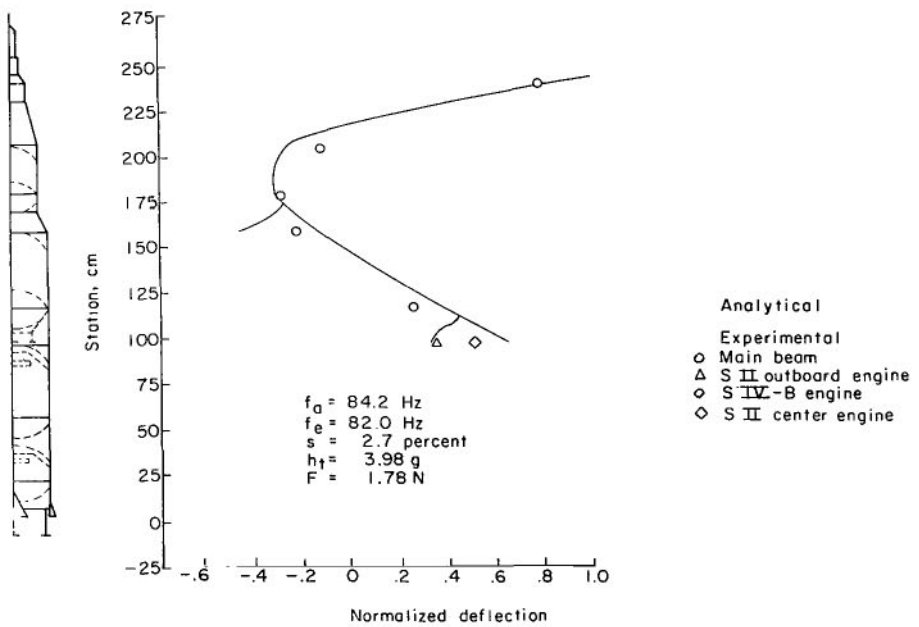

Figure 17.- Analytical and experimental free-free mode shape for configuration II without launch escape system. S-II stage empty and the S-IVB and Apollo 100 percent full.

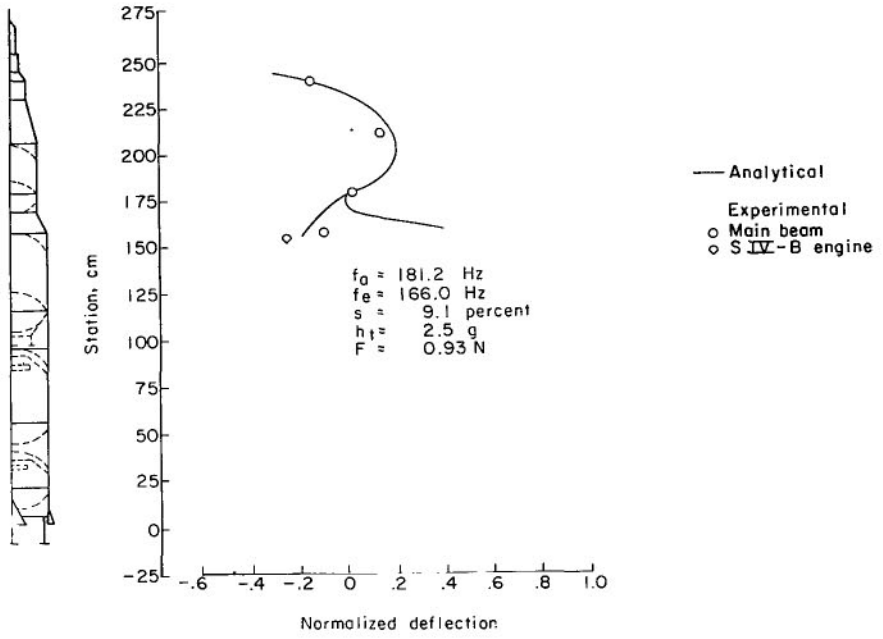

Figure 18.- Analytical and experimental free-free mode shape for configuration III. S-IVB and Apollo 100 percent full.

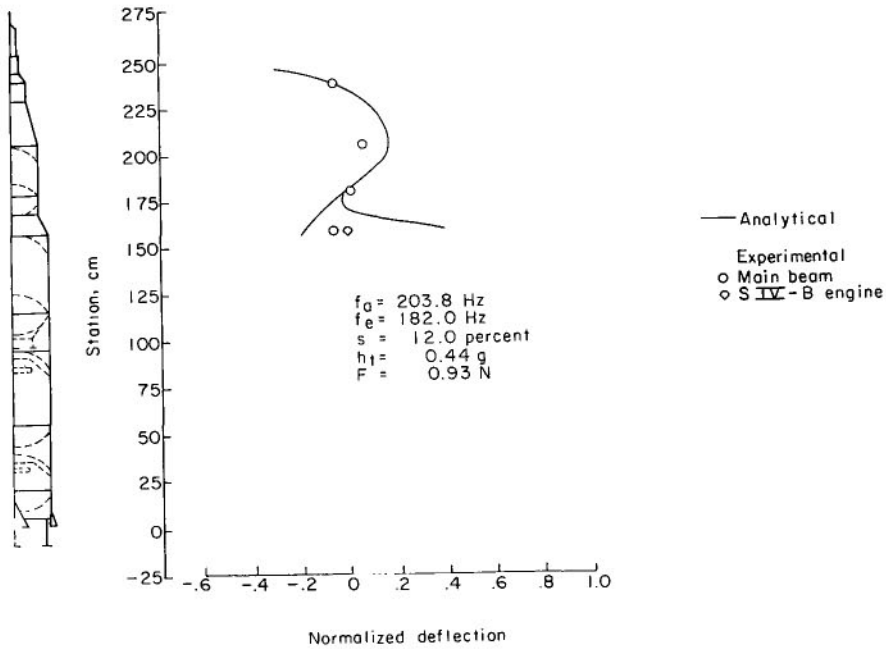

Figure 19.- Analytical and experimental free-free mode shape for configuration III. S-IVB empty and Apollo 100 percent full.

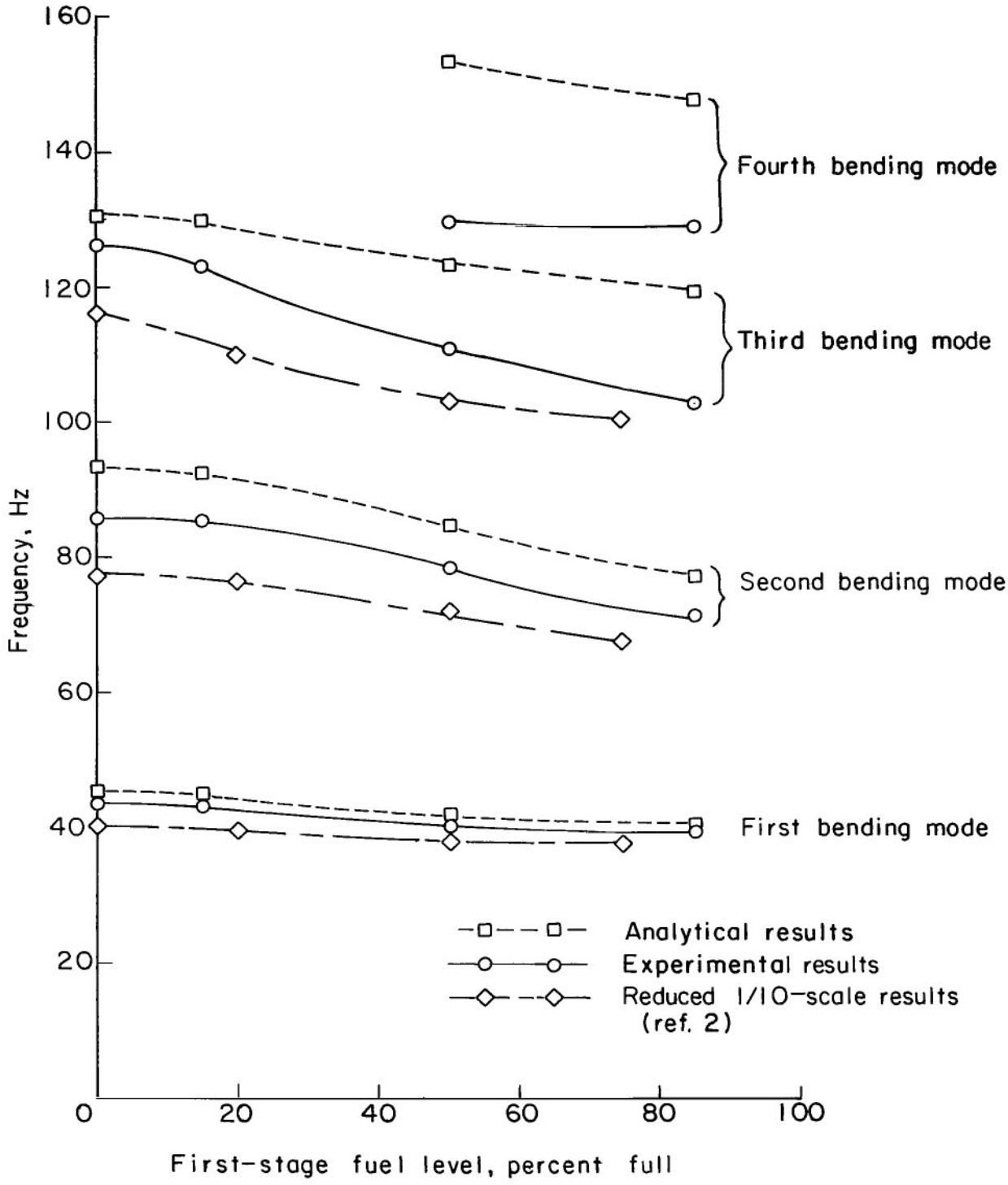

Figure 20.- Variation of the free-free bending frequency with the first-stage fuel level. Upper stages full.

NATIONAL AERONAUTICS AND SPACE ADMINISTRATION
WASHINGTON, D.C. 20546

OFFICIAL BUSINESS

FIRST CLASS MAIL

POSTAGE AND FEES PAID
NATIONAL AERONAUTICS AND
SPACE ADMINISTRATION

POSTMASTER: If Undeliverable (Section 158 Postal Manual) Do Not Return

"The aeronautical and space activities of the United States shall be conducted so as to contribute . . . to the expansion of human knowledge of phenomena in the atmosphere and space. The Administration shall provide for the widest practicable and appropriate dissemination of information concerning its activities and the results thereof."

—NATIONAL AERONAUTICS AND SPACE ACT OF 1958

NASA SCIENTIFIC AND TECHNICAL PUBLICATIONS

TECHNICAL REPORTS: Scientific and technical information considered important, complete, and a lasting contribution to existing knowledge.

TECHNICAL NOTES: Information less broad in scope but nevertheless of importance as a contribution to existing knowledge.

TECHNICAL MEMORANDUMS: Information receiving limited distribution because of preliminary data, security classification, or other reasons.

CONTRACTOR REPORTS: Scientific and technical information generated under a NASA contract or grant and considered an important contribution to existing knowledge.

TECHNICAL TRANSLATIONS: Information published in a foreign language considered to merit NASA distribution in English.

SPECIAL PUBLICATIONS: Information derived from or of value to NASA activities. Publications include conference proceedings, monographs, data compilations, handbooks, sourcebooks, and special bibliographies.

TECHNOLOGY UTILIZATION PUBLICATIONS: Information on technology used by NASA that may be of particular interest in commercial and other non-aerospace applications. Publications include Tech Briefs, Technology Utilization Reports and Notes, and Technology Surveys.

Details on the availability of these publications may be obtained from:

SCIENTIFIC AND TECHNICAL INFORMATION DIVISION

NATIONAL AERONAUTICS AND SPACE ADMINISTRATION

Washington, D.C. 20546